Hydrogen-Bonding and van der Waals Complexes Studied by ZEKE and REMPI Spectroscopy

Caroline E. H. Dessent† and Klaus Müller-Dethlefs*

Department of Chemistry, University of York, Heslington, York, YO10 5DD, U.K.

Received December 23, 1999

Contents

I. Introduction

The idea that molecules repel each other at small separations while attracting each other at long range was developed in the second half of the 19th century and first stated clearly by Clausius in 1857.[1] Intermolecular forces were subsequently incorporated into descriptions of the kinetic behavior of gases by Maxwell[2] and by Boltzmann.[3] In 1873, van der Waals postulated an equation of state for a gas whose molecules exerted an attractive force field at long range.[4] This equation was important since it predicted that pure substances can display gas−liquid transitions and critical points, and therefore demonstrated that the existence of the condensed phase arises from the attractive forces between molecules.

Contemporary research into molecular interactions aims at obtaining accurate intermolecular potential-energy surfaces through a combination of experiment and theory.[5−9] Within this area of research, molecular clusters are useful model systems for investigating intermolecular forces, which also operate in bulk systems, and have been actively studied over the last 25 years since investigations of these systems can yield high-resolution spectroscopic data and be treated with state-of-the-art theory. For closed-shell systems in their electronic ground states, the goal of obtaining spectroscopically accurate potential surfaces has recently been achieved for several systems including Ar_2•DCl and $(H_2O)_2$,[6,7] but the situation is quite different for ionic clusters. Progress in this area has been hampered by the experimental challenge of producing sufficient quantities of ionic complexes under the molecular beam conditions which are crucial for performing high-resolution spectroscopy. The detailed characterization of ion−solvent interactions is clearly an important goal, since they control fundamental chemical processes such as the dissolution of salts.

Zero-electron kinetic-energy (ZEKE) photoelectron spectroscopy is one of the spectroscopic techniques that has greatly contributed to improve our knowledge of the (ro)vibronic structure of cationic molecular complexes. Benzene•Ar and phenol•H_2O were the first van der Waals (vdW) and hydrogen-bonded complexes, respectively, to be studied using ZEKE spectroscopy.[10,11] Unlike traditional photoelectron spectroscopy, the technique offers sufficient spectral resolution to allow the identification of the low-frequency intermolecular modes in the ionic complex which characterize the vdW potential-energy surface. (The reader is referred to a number of reviews in this volume for other recent advances in spectroscopic studies of cationic complexes.) Since its introduction in 1984,[12] the ZEKE technique has been reviewed in

* To whom correspondence should be addressed. Telephone: (44 1904) 434526. Fax: (44 1904) 434527. E-mail: kmd6@york.ac.uk.
† Telephone: (44 1904) 434525. Fax: (44 1904) 432516. E-mail: ced5@york.ac.uk.

10.1021/cr990060r CCC: $35.00
Published on Web 09/14/2000

Caroline Dessent was born in 1969 in Gilfach Goch, Wales. She received her M.A. degree in Chemistry from Jesus College, Oxford University in 1991 and obtained her Ph.D. degree from Yale University in 1997. Her work on the structure and dynamics of dipole-bound excited states of anion–molecule clusters with Professor Mark A. Johnson was awarded the Richard Wolfson Dissertation Prize. Following her Ph.D. studies, she worked as a postdoctoral associate with Professor Klaus Müller-Dethlefs at the University of York on REMPI, ZEKE, and MATI spectroscopy of molecular clusters. In October 1999, she was awarded a Royal Society University Research Fellowship to continue her work at York. Her interests are in the spectroscopic characterization of ion-pair states of molecular complexes and experimental and computational studies of negative-ion systems.

Klaus Müller-Dethlefs was born in 1950 in Wilster, Germany. After studying chemistry and physics at the University of Göttingen, he received his Ph.D. degree in 1979 at Imperial College from the University of London for his work on soot formation with F. Weinberg, supported by a stipend from the Evangelisches Studienwerk Villigst. With a research fellowship of the Deutsche Forschungsgemeinschaft, he worked with J. P. Taran at ONERA (Châtillon, France) on coherent anti-Stokes Raman scattering (CARS) in flames. At the Institut fur Physikalische und Theoretische Chemie der Technischen Universitat München, he established the ZEKE method with its new applications in chemistry. Müller-Dethlefs was granted his habilitation in Chemistry in 1991, and in 1994 he received the Rudolf-Kaiser-Preis of the Stiftungsverband für die Deutsche Wissenschaft in recognition of his development of ZEKE spectroscopy. In 1995 he was appointed to the Chair of Physical Chemistry in the Department of Chemistry, The University of York, England. He held guest professorships at the Université de Bourgogne, Dijon, 1985, at Laboratoire Amié Cotton, Orsay, 1992, at the University of Atomic and Molecular Sciences, Taipeh, Taiwan, 1998, and at the Institute for Molecular Sciences, Okazaki, Japan, 1999. He has been chairperson of several international conferences. Recently, he was awarded the Tilden Lectureship 2000/2001 by the Royal Society of Chemistry. He is the first recipient of the Herzberg Memorial Prize and Fellowship of the National Research Council of Canada.

a number of articles,[13−22] and this review will therefore focus on its application to vdW complexes over the last five years.

Resonance-enhanced multiphoton ionization (REMPI) spectroscopy provides spectroscopic information on the excited states of neutral systems.[22−27] The technique is considered in this review along with ZEKE spectroscopy for two reasons. First, the two spectroscopies have frequently *both* been applied to the chemical systems we consider and provide complementary chemical information on the structure (and occasionally the dynamics) of the molecular cluster. Second, ZEKE spectra are often recorded using two-photon excitation, where the first photon accesses an intermediate electronic state of the neutral system and a second photon effects ionization. This approach has many benefits including (i) facile generation of the laser photons if ionization is achieved in this two-step approach, (ii) state selection of a specific molecular cluster so that the resulting ZEKE spectrum is not contaminated by coincidentally overlapping signal which results from an entirely different cluster, (iii) improved spectral resolution, and (iv) the opportunity to gain a fuller picture of the ionic potential-energy surface by effecting ionization via different intermediate states. Furthermore, the REMPI scheme is central to IR−UV double-resonance spectroscopies which have recently provided a wealth of information on vdW and hydrogen-bonded complexes.[28−30]

In this report, we review the application of REMPI and ZEKE spectroscopy to molecular complexes and trace the evolution of molecular interactions from complexes which are bound only by dispersion forces (e.g., Ar_2) to systems which contain strong hydrogen bonds (e.g., resorcinol·H_2O). Although hydrogen bonding is sometimes classified as vdW bonding, we distinguish it on the grounds of its strength compared to other intermolecular forces. Hydrogen bonds generally occur in systems, X−H···Y, where both X and Y are electronegative groups and Y possesses at least one lone pair of electrons (Y can also be the π-electrons of an unsaturated system). The interaction is directional and dominates all other vdWs interactions when it can occur. In this review, we extend this definition to include complexes where Y is an atom or molecule which binds to an X−H group with a geometry characteristic of a more traditional hydrogen bond *and* adopts this position in preference to an alternative vdW binding site. In section IV.B.i, for example, we discuss the phenol·Ar complex where the rare-gas atom can bind either above the aromatic ring at a vdW binding site (Figure 1a) or in the aromatic plane to the OH group, a hydrogen-bonding site (Figure 1b).

II. Experimental Methods

A. REMPI Spectroscopy

The REMPI process occurs by a resonant m-photon excitation from a ground electronic state molecule or cluster to an excited, (ro)vibronic state. One or more (n) additional photons are then absorbed and the molecule is ionized. The probability of ionization is enhanced by the fact that the first m photons are resonant with an intermediate state. This resonant ionization is abbreviated to $(m + n)$ R$(m + n)$PI for one-color and $(m + n')$ R$(m + n')$PI for two-color

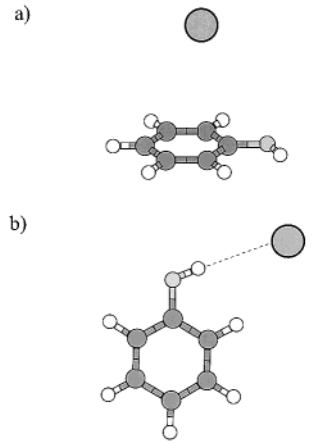

Figure 1. Schematic diagram illustrating (a) the vdW and (b) the hydrogen-bonded isomers of phenol·Ar.

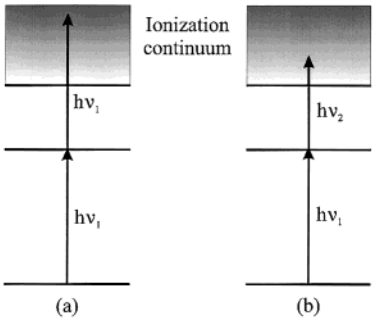

Figure 2. (a) One-color (1+1) and (b) two-color (1+1′) REMPI schemes.

photoionization. Most commonly used is resonance-enhanced two-photon ionization, termed (1 + 1′) R2PI. Figure 2a illustrates the case where the two photons have the same wavelength; a case described as (1 + 1) R2PI. While this method is popular due to the fact that it requires only a single dye laser, two-color (1 + 1′) R2PI (Figure 2b) should generally be preferred for studies of vdW complexes since the energy of the ionizing photon can then be lowered to reduce the probability of cluster fragmentation. This point is illustrated in Figure 3 for the REMPI spectrum of phenol·N_2 where the (1 + 1) R2PI spectrum (Figure 3a) is contaminated by fragmentation from higher mass channels into the mass channel which is being scanned (amu = 122).[31] This fragmentation is clearly suppressed by the use of the two-color (1 + 1′) R2PI ionization scheme (Figure 3b). The two-photon REMPI schemes illustrated in Figure 2 are the most common versions of REMPI for the vdW systems discussed in this review, although the method is, of course, not limited to two-photon processes.

The great advantage of the REMPI technique for investigating vdW complexes formed by a supersonic jet expansion, compared to other approaches such as laser induced fluorescence (LIF) which provide the same spectroscopic information, is its mass selectivity. The final-state ions can be readily detected in a time-of-flight spectrometer, allowing a mass-selective REMPI spectrum of one complex to be recorded without interference from other complexes. In addition, the technique is also species-selective due to the spectroscopic selectivity of the initial absorption

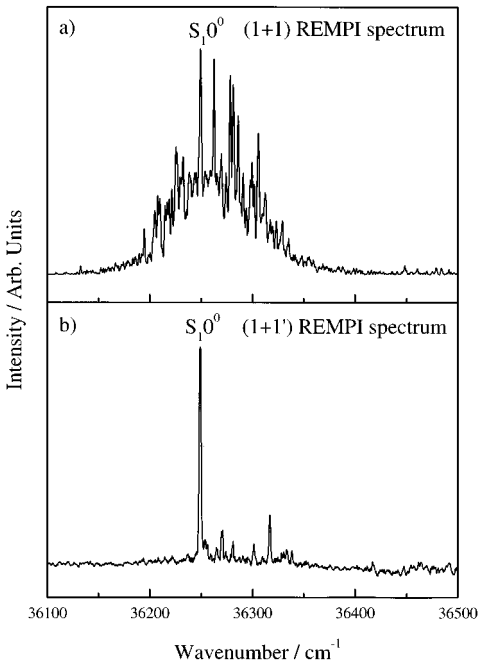

Figure 3. (a) One-color (1+1) and (b) two-color (1+1′) REMPI spectra acquired in the amu = 122 mass channel. The two-color spectrum, which was obtained with the ionization photon set to 31 521 cm^{-1}, represents the phenol·N_2 S_1 spectrum, while the one-color spectrum is contaminated by fragmentation from higher clusters. (Reprinted with permission from ref 31. Copyright 1998.)

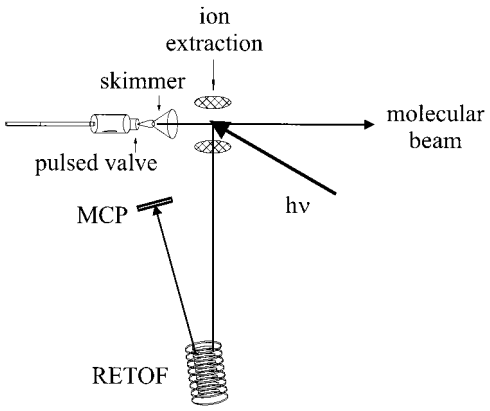

Figure 4. Schematic apparatus for REMPI spectroscopy with a reflectron mass spectrometer to achieve optimum mass resolution.

which will be molecule or cluster specific. This allows us to distinguish REMPI spectra of systems which have the same mass, e.g., phenol·N_2 and phenol·CO (see section IV.B.ii).

Figure 4 displays a schematic diagram of an experimental setup for REMPI spectroscopy. A basic apparatus consists of a laser system and a vaccum apparatus comprising a molecular-beam source, ion extraction plate, time-of-flight mass spectrometer, and multichannel plate detector. Although the simplest REMPI setup would involve linear time-of-flight analysis, a significant improvement in mass resolution is achieved with a reflectron time-of-flight (RETOF) mass spectrometer.[32] In a typical two-color experiment, both dye lasers are pumped simultaneously by either an excimer or an Nd:YAG laser. After ionization, an extraction pulse is applied and

the ions are detected with multichannel plates. Spectra are then acquired by setting narrow time gates and monitoring ion signal intensity as a function of photon energy with a boxcar integrator or digitizing oscilloscope.

High-resolution REMPI spectroscopy aims to resolve individual rotational transitions in addition to vibrational features.[33,34] By employing a skimmed supersonic molecular beam, the transverse velocity distribution and consequently the Doppler width is reduced to a level where rotationally resolved spectra can be obtained if narrow bandwidth lasers are used. Spectral resolution on the order of 100 MHz has been obtained in a (1 + 1′) REMPI experiment using a pulsed amplified cw laser with a bandwidth of 60 MHz for S_1-S_0 excitation. The ionization laser used was a broad-band XeCl excimer pumped dye laser. This approach has allowed the acquisition of fully rotationally resolved REMPI spectra of several vdW complexes.[33,34] We note that comparable resolution has also been obtained in LIF spectroscopy,[35,36] which provides the same spectroscopic information as REMPI but without mass resolution.

B. ZEKE Spectroscopy

ZEKE spectroscopy is a modification of the well-known photoionization technique, photoelectron spectroscopy (PES).[37,38] In PES, a high-energy photon source ionizes a sample and the kinetic energy of the resulting photoelectrons is analyzed to reveal the energy levels of the corresponding ion. The resolution of PES is limited for a number of technical reasons to ca. 10 meV (80 cm^{-1}),[39] which is problematic if we hope to study vdW vibrational modes which can display frequencies on this order of magnitude. Threshold photoelectron spectroscopy (TPES) was subsequently introduced in an attempt to improve the resolution of traditional PES by selecting photon energies so that electrons are emitted only at the threshold of a specific ionic eigenstate.[40,41] The resulting photoelectrons possess very low kinetic energies and can be discriminated from higher kinetic-energy electrons which are produced as the photoexcitation laser is scanned between the ionic eigenstates.

ZEKE spectroscopy differs from both PES and TPES in that ionization is achieved in two distinct, successive stages. First, the system is photoexcited to a high-*n* Rydberg state, and then after a time delay of several microseconds, field ionization of the prepared Rydberg state is induced by a pulsed electric field. This process has led to ZEKE spectroscopy being more fully described as ZEKE-pulsed field ionization (ZEKE-PFI), although we adopt the shorter notation in this review. A ZEKE spectrum is then acquired by measuring the yield of electrons produced by delayed PFI as the photoexcitation laser is scanned across successive ionization thresholds. The best resolution obtained by ZEKE spectroscopy to date is about 0.15 cm^{-1},[42] close to the bandwidth of typical dye lasers.

The success of ZEKE spectroscopy relies on the properties of the high-*n* Rydberg states ($n > 150$) which exist in a very narrow band just below the ionization threshold of each ionic eigenstate. These states display a stability which is entirely unexpected from the n^3 scaling law that applies to the lifetimes of lower-*n* Rydberg states.[43] Therefore, these high-*n* states can be separated from the fast decaying low-*n* Rydberg states by simply using a delay period prior to ionization. Since the electron, although spatially diffuse, is still associated with the ion core, the system remains neutral and can be efficiently separated from ionized states.

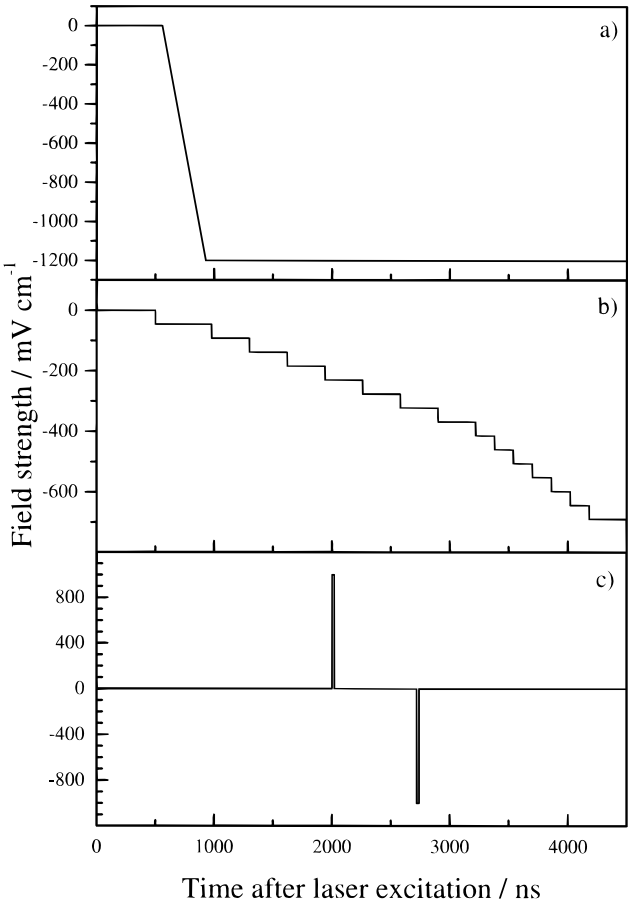

Figure 5. Tailored pulses employed to improve ZEKE spectral resolution: (a) sloping pulse, (b) staircase pulse, and (c) fractional Stark-state field ionization pulse.

The stability of the high-*n* Rydberg states has been found to arise from external perturbations which are most significant for these states. In ZEKE spectroscopy, external fields are now understood to produce the long lifetimes by effecting Stark mixing of orbital angular momentum l and its projection m_l in the high-*n* region.[44] (Large concentrations of photoions can also induce Stark-state mixing and produce the same effect.[45]) It is now possible to selectively manipulate the lifetimes and stability of Rydberg states which lead to ZEKE electrons by a careful application of externally applied pulsed fields.[46,47]

Several field ionization pulse schemes have been introduced which allow basic ZEKE spectral resolution to be further improved. One technique employs various sloping pulses.[48] A fast pulse will generate the entire ZEKE signal within a narrow TOF distribution, while a more slowly rising pulse (Figure 5a) spreads different "slices" of Rydberg electrons into a broader TOF distribution. A smaller spectral "Ryd-

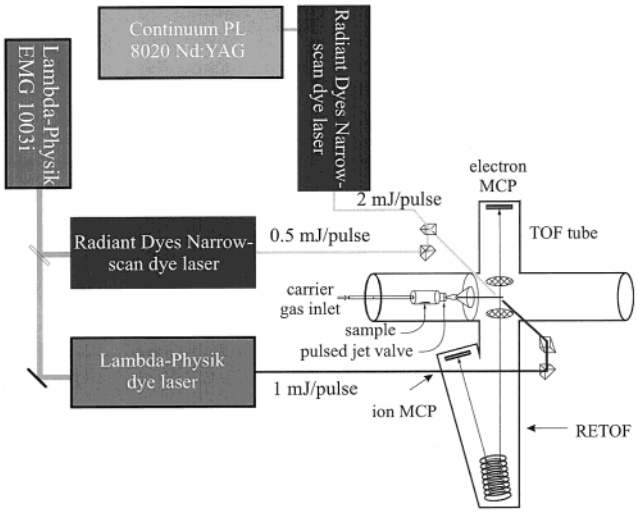

Figure 6. Schematic diagram of an experimental apparatus for ZEKE spectroscopy. The pump and probe lasers counter-propagate into the ionization region, and a third laser can be introduced collinear with the pump laser through a beam splitter to conduct hole-burning spectroscopy.

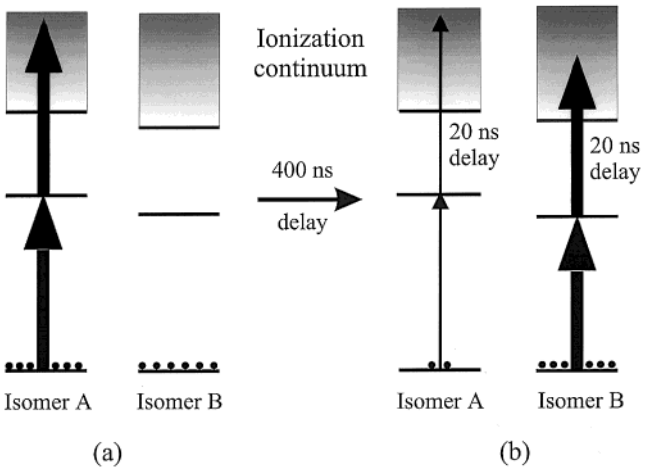

Figure 7. Energy-level diagram for hole-burning spectroscopy. A high-intensity laser depopulates isomer A via resonance with an S_1 intermediate state. A second laser is introduced sometime later and probes the ground state of isomers A and B, which is detected via ionization through a one-color REMPI process. Due to the depopulation of isomer A, the signal from transitions involving isomer A are reduced compared to transitions corresponding to isomer B.

berg slice" can then be acquired by setting a narrow TOF gate. Multistep staircase pulse schemes (Figure 5b) are a close variation on the sloping pulse scheme, although they offer the further advantage of allowing an exact determination of the field-free ionization energy by extrapolation.[49] The best ZEKE spectral resolution to date was demonstrated by Dietrich et al. in 1996 using an inversion of the orientation of two field pulses to selectively ionize "red" and "blue" Stark states.[42] In this method, termed fractional Stark-state field ionization (FSSFI), a first electric pulse preferentially ionizes the red Stark states while some of the blue (higher energy) states survive until a second pulse is applied in the opposite direction, shifting the blue states to lower energies (Figure 5c). The offset-to-probe ratio of the pulsed electric field can be tuned to produce optimum ZEKE resolution.

A schematic representation of an experimental setup for ZEKE spectroscopy used at York is shown in Figure 6. The apparatus consists of a synchronously pumped double dye laser system and a vacuum apparatus that contains a molecular-beam source, extraction plates, and a μ-metal shielded flight tube with a multichannel plate electron detector. A RETOF mass spectrometer is positioned at 180° to the electron flight tube in a configuration that allows mass-analyzed threshold ion (see section III.B) signal to be obtained simultaneously with ZEKE electron signals.[50,51]

III. Techniques Employing REMPI and ZEKE Spectroscopy

A. Hole-Burning Spectroscopy

van der Waals complexes can be mass analyzed using ionization techniques such as REMPI, which allow the acquisition of spectra due to a single cluster mass. However, a further problem exists, since the mass alone does not uniquely specify a complex, which may occur as several structural isomers. Such isomers can be distinguished using spectrally resolved hole-burning spectroscopy. Hole burning was first coupled with REMPI spectroscopy in a supersonic jet by Lipert and Colson to test if multiple isomers are present in the REMPI spectrum of phenol·H_2O,[52] although Scherzer et al.[53] were the first to actually observe multiple isomers in the benzene·Ar_2 complex.[54] Hole burning (using both UV and IR hole-burning photons) has now been widely applied with REMPI spectroscopy[28,29,30,52,53,55−61] and has even been used to distinguish enantiomeric complexes.[62,63]

The idea behind hole-burning experiments is that lasers are capable of depleting the population of a molecule or complex when the laser is resonant with a spectral transition of that species. For most molecular complexes and polyatomic molecules, the relaxation rate to re-populate the initial state is sufficiently slow that if a second probe laser is applied sometime after the hole-burning laser, a reduction in intensity of all transitions originating in the species that was in resonance with the first laser is observed. Figure 7 illustrates the application of hole burning to one-color (1 + 1) REMPI spectroscopy. However, it is also possible to apply hole-burning spectroscopy to two-color (1 + 1′) REMPI spectroscopy, and this is desirable for vdW complexes, e.g., phenol·H_2O·Ar,[64,65] where one-color REMPI leads to fragmentation of the weakly bound complex.

An example of the application of hole-burning spectroscopy is shown in Figure 8. The (1 + 1) REMPI spectrum of the resorcinol·CO complex is displayed in Figure 8a. The prominent bands at 35 808 and 36 100 cm^{-1} were assigned to the origin transitions of two rotational isomers of the resorcinol·CO complex (Figure 31). Hole-burning spectroscopy was conducted to confirm this assignment, and Figure 8 parts b and c show the spectra obtained with the hole-burning laser set to the two respective $S_1$0° transitions. In Figure 8b, the hole-burning laser was

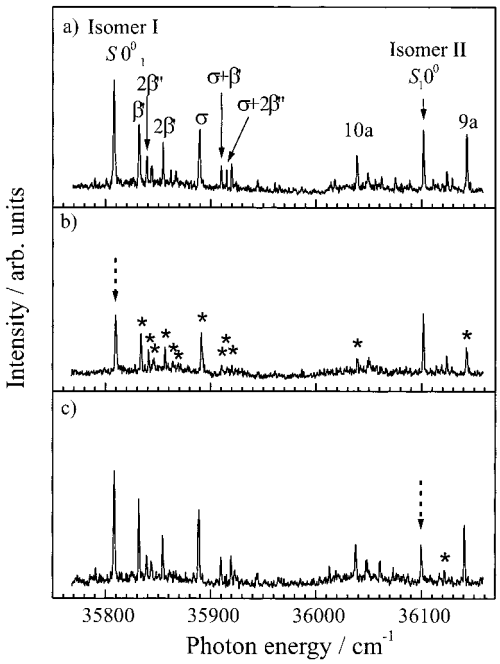

Figure 8. Hole-burning spectra of resorcinol·CO with (a) no hole-burning laser (one-color REMPI spectrum), (b) the hole-burning laser set to $S_1 0°$ of isomer I, and (c) the hole-burning laser set to the $S_1 0°$ transition of isomer II. The hole-burning laser position is marked with the dashed arrows, and bands affected are marked with asterisks. (Reprinted with permission from ref 61. Copyright 1999 American Chemical Society.)

set to the isomer I $S_1 0°$ transition. The spectrum clearly indicates that two distinct species are present in the REMPI spectrum since the isomer II $S_1 0°$ transition is unaffected by the burn laser. This result is confirmed by the spectrum presented in Figure 8c, where the burn laser was set to the $S_1 0°$ transition of isomer II. Vibrational features associated with the two S_1 origins are also selectively depleted in the two hole-burning spectra. The presence of two rotational isomers was confirmed by obtaining ZEKE spectra *via* each $S_1 0°$ intermediate state.[61]

B. Mass-Analyzed Threshold Ionization Spectroscopy

Mass-analyzed threshold ionization (MATI) spectroscopy was suggested by Zhu and Johnson in 1991 as a variation of the ZEKE method that allows mass analysis of ions produced by pulsed field ionization.[66] This technique is particularly useful for studying molecular complexes since it facilitates unambiguous identification of the ionized species and can therefore be used to follow reactive processes such as cluster fragmentation.[33,67−69]

Until recently, the resolution of the MATI technique has suffered compared to ZEKE spectroscopy since relatively large separation fields and field ionization pulses have been employed to separate PFI ions from 'spontaneous' ions produced by the initial laser pulse.[51] A new scheme has recently been developed which uses FSSFI[42] to maximize the MATI experimental resolution and allows MATI spectra to be obtained with identical resolution to ZEKE spectra.[50] The key to the new scheme lies in a careful

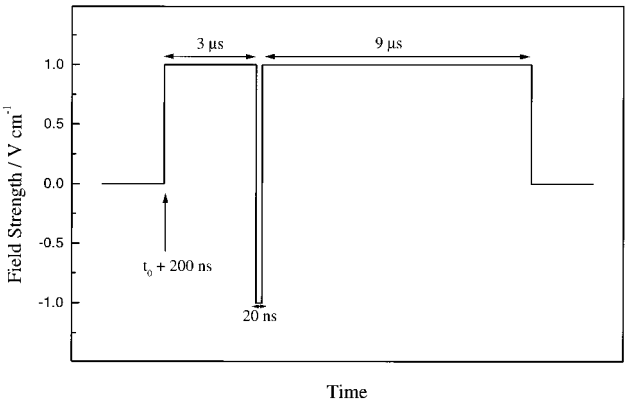

Figure 9. Tailored pulse used to obtain high-resolution MATI spectra. See text for details.

choice of the field ionization pulse. Figure 9 displays an example of a tailored pulse that has been employed to obtain high-resolution MATI spectra of phenol·Ar. The excitation lasers fire at $t = 0$, followed by the application of a +1 V/cm pulse 200 ns later on. This pulse can be considered to be equivalent to the separation pulse employed in a typical MATI experiment but will also ionize the more fragile "red" Stark states. The more resilient "blue" states survive, and the spontaneous ions spatially separate from the neutral Rydberg states for 3 μs before the electric field is rapidly inverted to −1 V/cm for 20 ns. Stark-state inversion occurs, and the original "blue" states are now ionized, producing high-resolution ZEKE electrons and MATI ions. The polarity of the electric field is now reversed again to continue the spatial separation of spontaneous ions from both the high-resolution MATI ions and the remaining Rydberg states which will be ionized to produce low-resolution MATI signal by the substantial pulsed field (290 V/cm) used to extract ions into the RETOF analyzer. Although the inverted 20 ns pulse reverses the field experienced by the spontaneous ions, and therefore counteracts the spatial separation achieved during the first 3 μs, the effect is only marginal due to the shortness of this pulse.

Synchronous ZEKE and MATI spectra of the phenol·Ar complex recorded using the new detection scheme are presented in Figure 10. The low-resolution MATI spectrum (Figure 10c) can be regarded as a rather typical example and clearly illustrates the poor resolution of the method compared with ZEKE spectroscopy (Figure 10a). The doublet feature centered at 29 cm^{-1} ion internal energy merges into a single feature, while the peak at 37 cm^{-1} ion internal energy is entirely obscured compared to the ZEKE spectrum. However, the resolution of the high-resolution MATI spectrum (Figure 10b) compares extremely well with the ZEKE spectrum, a result which is entirely expected since *the two spectra arise from ionization of the same Rydberg states*. The fwhm of the IE peak in the low-resolution MATI spectrum (Figure 10c) is 6 cm^{-1}, while the fwhm of the corresponding peak in the high-resolution MATI spectrum (Figure 10b) is 3 cm^{-1}. This value is indeed equal to the fwhm of the IE peak in the ZEKE spectrum (Figure 10a) which is also 3 cm^{-1}.

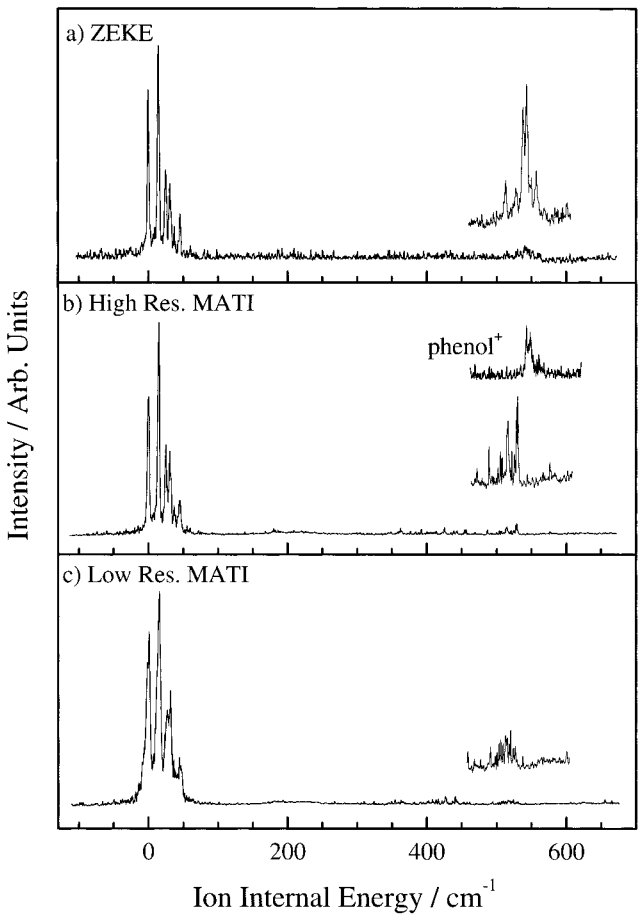

Figure 10. Synchronously recorded (a) ZEKE, (b) high-resolution MATI, and (c) low-resolution MATI spectra of phenol·Ar recorded via the $S_1 0°$ band origin. The spectra are enlarged over the region of the dissociation threshold, and the phenol$^+$ daughter fragment spectrum is included on b. (Reprinted with permission from ref 50. Copyright 1999.)

Inspection of the spectra over the region 450−600 cm^{-1} ion internal energy reveals that while the MATI signal ends abruptly above ∼530 cm^{-1} due to dissociation of the ionic core, the ZEKE signal continues. The high-resolution MATI spectrum of the daughter fragment, phenol$^+$, is included in Figure 10b. An analysis of the spectra gives the [phenol·Ar]$^+$ dissociation energy as 535 ± 3 cm^{-1}. Note that unlike previous MATI dissociation spectra,[67,70] there is *no overlap of signal between the parent and daughter mass channels*, probably due to the small electric field employed to ionize the Rydberg states (1 V/cm versus ∼500 V/cm). This experiment illustrates that there is no reason to believe that the signal will always overlap between the parent and daughter channels due to energy transfer from electronically excited high *n*-Rydberg electrons to the vibrational degrees of freedom of the ionic core, as suggested previously.[70] In light of the present results, this observation can now be understood as an artifact due to the lower-*n* Rydberg states employed in that high-field experiment. For those lower-*n* Rydberg states, the electron still interacts with the ion core and the field can influence the electron−core coupling.

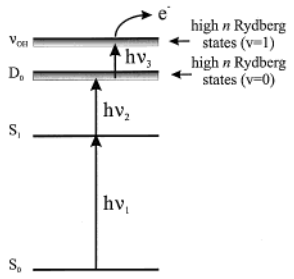

Figure 11. Energy levels involved in PIRI spectroscopy.

C. Photoinduced Rydberg Ionization

ZEKE and MATI spectroscopy have generally been applied to the ground electronic states of cations since very high photon energies would be needed to access cationic excited states. In addition, the lifetimes of such core excited states may be too short to allow ZEKE spectra to be recorded. To surmount these problems, a new technique termed photoinduced Rydberg ionization (PIRI) spectroscopy was introduced by Johnson and co-workers in 1995.[71,72] The technique uses the fact that a Rydberg electron interacts very little with optical radiation and, therefore, the absorption cross-section of a Rydberg state is approximately the same as that of the core ion. The PIRI technique first produces high *n*-Rydberg states, and then an additional photon is introduced to promote a core electronic transition which can lead to rapid autoionization (Figure 11), producing ions which can be detected in a mass spectrometer.

It should be noted that the PIRI technique relies on some interaction of the Rydberg electron with the ion core, and hence, the principal quantum number must not be too high. On the other hand, the lower-*n* states have shorter lifetimes and, due to the interaction of the electron with the core, might not be fully representative of an unperturbed ion core. From a practical point of view, it is easiest to carry out PIRI experiments in the presence of large ion concentrations. The perturbation of the Rydberg states by the ions results in lifetime stabilization of the $100 < n < 150$ states by l and m_l mixing. Since the l and m_l mixing implies that the electron can return to low l and hence interact with the core, the Rydberg states have a nonzero probability to autoionize upon photoexcitation of the ion core: this autoionization is detected as PIRI signal.

In the original experiment, electronic transitions in the benzene cation were probed optically. This approach was later extended by Fujii et al. who used infrared photons to monitor vibrational transitions of a phenol ion core through autoionization of high-Rydberg states.[73] They called this method autoionization-detected infrared spectroscopy (ADIR). Gerhards et al. very recently used the same basic scheme but with the refinement that ionic vibrations are detected via depletion of a MATI signal.[74] This has the advantage over ADIR that weaker combination modes of the ion can be detected in depletion when they would not be observable as an increase in the spontaneous ion signal. While these techniques have only been applied to isolated monomers to date, they clearly represent useful tools for studying cationic

above-ring complexes. It is particularly worth noting that direct infrared spectroscopy of the ion core provides an excellent complement to ZEKE spectroscopy for which the Franck−Condon factors are frequently extremely weak over the spectral region where high-frequency vibrational modes appear.

D. IR–UV Double Resonance

One of the most powerful spectroscopic probes of hydrogen-bonding networks is the OH stretch region of the infrared. The vibrational frequency and IR intensity of the OH stretch fundamentals are sensitive functions of the number, type, and strength of hydrogen bonds in which each OH group participates. The coupling of IR−UV double-resonance spectroscopy, which developed from earlier double-resonance spectroscopies,[75−77] has proved a powerful spectroscopic tool for studying the IR spectra of neutral and cationic complexes.[28−30,58,78−82] Figure 12 illustrates the two experimental schemes used. To monitor the IR spectrum of a specific neutral complex, transitions are detected via depletion of the UV-laser-induced REMPI ion signal at the mass of the complex (Figure 12a). The IR pulse is applied before (50 μs to 100 ns) the UV pulse to restrict the IR depletion to the ground state of the probed species. This approach has been termed resonant ion-dip infrared spectroscopy (RIDIR) by Zwier and co-workers[28] and has been extremely successfully applied to study hydrogen-bonding species due to the IR intensity of OH/NH stretching vibrations. Alternatively (Figure 12b), IR spectra of cationic complexes can be obtained if the IR laser pulse is introduced shortly after the UV laser. Ions can be produced in their vibrational ground state via a two-color (1 + 1′) REMPI transition, and the cationic spectra can be recorded through detection of the vibrationally predissociated daughter fragment ion. Brutschy and co-workers employed this approach to monitor ion−molecule reactions in clusters.[83,84] Like REMPI spectroscopy, both approaches are ideally suited to studies of molecular clusters since they provide mass-selective analysis. Generally, Nd:YAG pumped optical parametric oscillators (OPO) have provided the IR photons in these experiments,

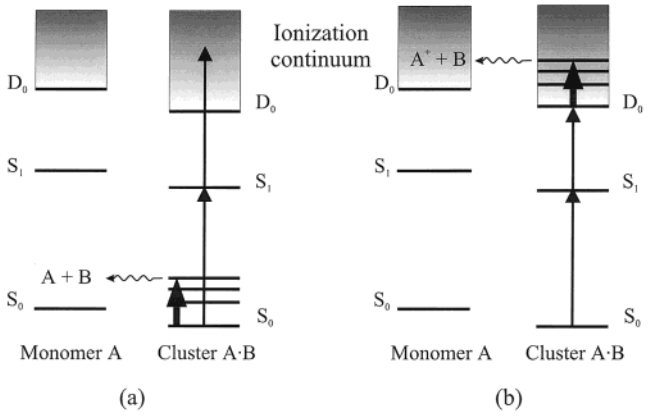

Figure 12. Energy levels involved in IR−UV double resonance; (a) The case where the IR laser is introduced before the UV lasers to acquire spectra of the neutral system. (b) The scheme where the IR laser is introduced after the UV lasers to record spectra of the cation.

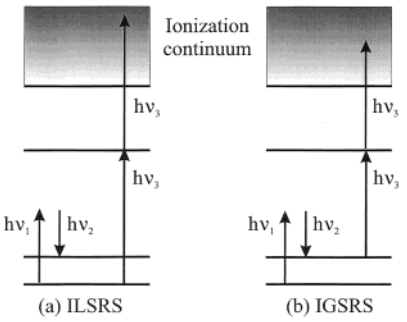

Figure 13. Energy levels involved in ionization-detected stimulated Raman spectroscopy. $h\nu_1$ and $h\nu_2$ drive a stimulated Raman transition, while $h\nu_3$ probes a REMPI transition either (a) as a signal depletion, ionization loss stimulated raman spectroscopy, ILSRS, or (b) as a signal gain, ionization gain stimulated raman spectroscopy, IGSRS.

although Meijer and co-workers recently used a widely tunable free-electron laser (FELIX) to obtain IR spectra over the 40−2000 cm^{-1} range.[81,82]

E. Stimulated Raman–UV Double Resonance

Stimulated Raman−UV double-resonance spectroscopy is very closely related to the IR−UV double-resonance techniques described in the previous section.[85,86] In this spectroscopy, vdW complexes in a molecular beam are efficiently excited to a vibrational level by stimulated Raman pumping. Either a depletion of the population of the vibrational ground state (IDSRS−Figure 13a) or an increase of the vibrationally excited cluster (IGSRS−Figure 13b) is monitored using a REMPI signal. The technique was first demonstrated on molecular clusters by Felker and co-workers, and the reader is referred to a previous review for a more detailed discussion of the method.[85] Naphthalene trimers have most recently been studied using this approach.[87]

F. Time-Resolved Studies

ZEKE spectra recorded via S_1 intermediate states have been used to monitor vibrational energy transfer in the S_1 state in an elegant series of experiments.[88−90] The basic approach uses a pump photon to excite an intramolecular vibration in the S_1 state of the vdW complex, and a subsequently applied probe (ionization) photon competes against the predissociation rate of the complex. The delay between the pump and probe lasers determines whether vibrations due to the complex or a dissociated daughter fragment is observed in the ZEKE spectrum. Energy transfer in fluorene·Ar$_n$ $n = 1-3$ complexes has most recently been investigated by Knee and co-workers[89] using this technique. For a more detailed discussion, we refer the reader to a recent review of chemical applications of ZEKE spectroscopy.[13]

A number of time-resolved studies employing REMPI detection have also been performed over recent years.[91−95] Reference 91 presents a review of work in this area. Particularly notable are the studies by Syage, Zewail, Castlemann, and co-workers on proton-transfer reactions in hydrogen-bonded clusters. In a typical pump−probe experiment, chemistry

is initiated in the S_1 state by a photoexcitation pulse and the evolution of cluster properties interrogated at later times by probe excitation with mass-resolved ion detection. A recent example is provided by the work of Kim et al.[93] on proton-transfer reactions in 1-naphthol·(solvent)$_n$ clusters, where $n = 1-21$ and the solvent used was either NH_3, H_2O, or piperidine. The rates and threshold for proton transfer were found to be critically dependent on the number and type of solvent molecules.

IV. Probing the Transition from van der Waals to Hydrogen Bonding: REMPI and ZEKE Spectroscopy of Molecular Complexes

A. Inorganic Complexes

i. $(Ar)_2$

A rare-gas dimer is an example of a complex that displays purely dispersion-induced van der Waals binding. The neutral ground state of $(Ar)_2$, like other rare-gas dimers, is repulsive at short internuclear distances but displays a shallow well at larger distances [$r_e(Ar)_2 = 3.759$ Å].[95] However, like excimer molecules, many of its electronic excited states display considerable bound character. Although these states are amenable to study using ZEKE spectroscopy as a result of their Rydberg character, poor Franck−Condon factors for direct excitation of the ground neutral state to these ionic states have been observed using HeI PES.[96] Clearly, $(Ar)_2^+$ will be much more strongly bound than the neutral dimer due to the ion-induced dipole interaction.

Signorell and Merkt[97] presented a detailed ZEKE-PFI study of the ground A $^2\Sigma^+_{1/2u}$ and excited C $^2\Pi_{\Omega u}$ ($\Omega = {}^1/_2, {}^3/_2$) states of Ar_2^+. The cation is accessed indirectly through channel couplings which allow measurements to be conducted on non-Franck−Condon-accessible vibrational states. An extensive vibrational progression was observed in the A state for $v^+ = 3-52$, and rotational constants were abstracted for several of these vibrational levels. These measurements allowed the derivation of an analytical potential-energy curve for the A $^2\Sigma^+_{1/2u}$ state which extends to large internuclear distances (>5 Å) and characterizes the long-range potential as the expected ion-induced dipole interaction.

ii. Ar·NO

Weakly bound complexes of small inorganic molecules with rare-gas atoms are of fundamental interest since these complexes represent prototypes for characterizing simple multipole-induced dipole interactions.[98−101] Clusters containing open-shell molecules, e.g. Ar·NO, have been of particular interest as the perturbation of the open-shell molecule by the rare-gas atom can be studied in detail by observing the coupling and quenching of angular momentum. A number of REMPI and ZEKE studies have been performed on Ar·NO, and the reader is referred to another review for a summary of results up to 1994.[12−14]

Bush et al.[98] recently performed a detailed REMPI and ZEKE study which has concentrated on the A $^2\Sigma^+$ state of the neutral. A simulation of the A $^2\Sigma^+-X$ $^2\Pi$ REMPI spectrum (using the rare-gas−open-shell molecule model of Hutson[102]) suggested that the ground vibrationless level of the A $^2\Sigma^+$ state has a linear geometry while some of the higher vibrational levels display a skewed T-shaped structure. This assignment was confirmed by obtaining ZEKE spectra via both sets of vibrations. Spectra recorded via the ground vibrationless level show progressions which correlate with transitions to highly excited vdW stretching and bending levels, while spectra recorded via intermediate levels with a T-shaped geometry show progressions which correlate principally with the vdW stretching mode. In both cases, no vibrational structure was detected close to the ionization threshold but peaks at higher excitation energy were observed, corresponding to high-lying vibrational levels of the Ar·NO^+ ion.

These observations were interpreted in terms of large changes in the intermolecular bond length and bond angle upon ionization and discussed in terms of the vdW interactions which are present in the neutral and cationic systems. Analysis of the vibrational levels of the A state indicate that the vdW bond is considerably longer than that calculated for Ar·NO^+, and the A state is therefore non-Rydberg in character. This behavior was attributed to the Ar atom being too large to fit within the average orbit of the NO 3sσ Rydberg electron. The spectra also reveal that Ar·NO adopts a linear geometry in the A state, indicating that dipole−induced-dipole and induced-dipole−induced-dipole forces dominate over the quadrupole−induced-dipole and exchange−repulsion interactions.

iii. $(NO)_2$

The neutral ground-state geometry of the NO dimer has been well established from microwave and infrared studies as a cis C_{2v} structure.[14] The first ZEKE spectrum of $(NO)_2$ was recorded by Fischer et al.[103] in 1992 and showed considerable vibrational structure which mainly consisted of a progression spaced by 118 cm^{-1}. This vibration was tentatively assigned as a torsional mode associated with ionization to a C_{2h} symmetry ion. (The one-color, nonresonant ZEKE spectrum is reproduced in Figure 14.) However, the FC distribution is not entirely consis-

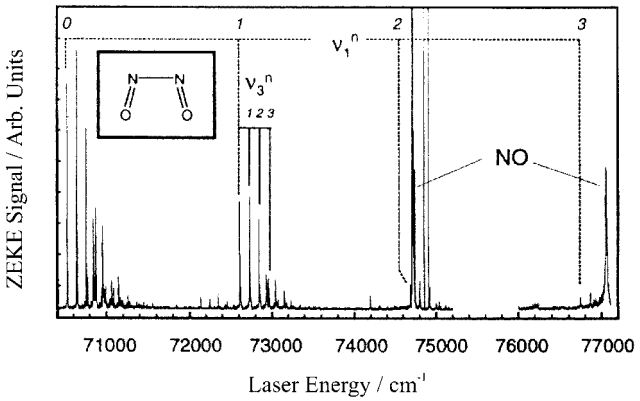

Figure 14. Nonresonant one-color ZEKE spectrum of $(NO)_2$ recorded by Fischer et al. (Reprinted with permission from ref 103. Copyright 1992.)

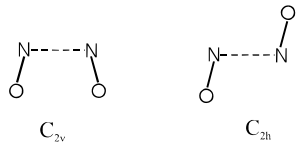

Figure 15. Schematic structures of $(NO)_2^+$ of C_{2v} and C_{2h} symmetry.

tent with a cis−trans isomerization. Strobel et al.[104] subsequently proposed that ionization accessed a trans−planar C_{2h} structure. More recently, Urban et al. obtained MATI spectra of the dimer and concluded that the photoelectron spectrum corresponds to cis−cis ionization.[105] Isomeric structures of $(NO)_2^+$ are illustrated in Figure 15.

A new, high-level ab initio study of $(NO)_2^+$ by Lee and Wright[106] has determined that the ground ionic state corresponds to the trans isomer, which has C_{2h} symmetry. The cis isomer was calculated to lie 100 cm^{-1} higher in energy at the RCCSD(T)/aug-cc-pVQZ-(no g)//UQCISD/6-311+G(3df) level of theory. (It should be noted that the NO dimer, in both its neutral and cationic states, presents a considerable challenge for theoretical study due to the unpaired electrons.) A reassignment of the ZEKE spectrum of $(NO)_2$ was suggested in light of the new calculations. Since the ground-state structure adopts a C_{2v} geometry, the vertical ionization should access the C_{2v} ionic minima. It then follows that the 118 cm^{-1} mode cannot be a torsional vibration and was therefore assigned to the N−N stretch which appears at 193 cm^{-1} at the ROHF/6-311+G(3df) level of theory. This assignment is persuasive since a cis−cis ionization is more consistent with the strong FC intensities observed in the ZEKE spectrum than a cis−trans ionization.

A second ab initio study by East and Watson[107] was published shortly after the report of Lee and Wright.[106] East and Watson also used RCCSD(T) theory and the aug-cc-pVDZ basis set to explore the structure of the electronic ground state of $(NO)_2^+$ and found that almost isoenergetic minima exist for the planar cis (C_{2v}) and trans (C_{2h}) geometries. These authors also concluded that the FC factors from the ground state of $(NO)_2$ should strongly favor vertical transitions to the cis isomer. A one-dimensional torsional FC analysis confirmed that the ZEKE spectrum corresponds to a cis−cis ionization.

iv. $(NH_3)_2$

The ammonia dimer has been investigated widely as a model system where a number of fundamental concepts can be studied, such as internal hydrogen-atom and proton transfer. Indeed, the spectroscopic characterization of the potential-energy surface of $(NH_3)_2$ has greatly contributed to our understanding of the dynamical structure of vdW complexes (see ref 5 for a review). To date there are no ZEKE spectroscopic studies of $(NH_3)_2$, possibly due to the fact that the complex experiences a substantial geometry change upon ionization, but we will discuss a recent femtosecond time-resolved photoelectron spectroscopy study of $(NH_3)_2$ by Hertel and co-workers here,[108] since it should be of interest to the reader.

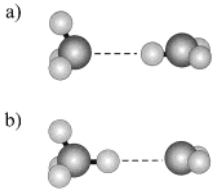

Figure 16. Schematic structures of $(NH_3)_2^+$. (a) The geometric structure accessed in a vertical transition from the neutral ground state of $(NH_3)_2$. (b) The ground state, cationic geometry, $NH_4^+ \cdot NH_2$.

The appearance potential of $(NH_3)_2^+$ has been identified previously[109] at 9.19 eV and is thought to correspond to a complex where one of the NH_3 molecules is prepared in its ionic ground state (a planar D_{3h} symmetry—Figure 16a). However, the energetically most stable configuration corresponds to a proton-transfer complex, $NH_4^+ \cdots NH_2$, which adopts a C_s symmetry structure (Figure 16b). In the work of Farmanara et al.,[108] the energy flow in $(NH_3)_2$ excited to the electronic A state was analyzed by combining femtosecond pump−probe techniques and photoelectron−photoion coincidence detection. The photoelectron spectra of $(NH_3)_2^+$ change drastically from a rather broad feature (>1 eV) at small pump−probe delay times to a narrow peak (0.25 eV) on a time scale of picoseconds. These observations were explained by a model where internal H-atom transfer occurs in the A state to an $NH_4 \cdots NH_2$ configuration, where the picosecond lifetime of the state is understood to arise from a conical intersection with the charge-transfer state $NH_4^+ \cdots NH_2^-$. These observations were supported by ab initio calculations (CASSCF-MRCI) which suggest that the charge-transfer and proton-transfer potential-energy surfaces are well characterized at the level of theory employed.

v. $Na \cdot H_2O$

Alkali metal ions solvated by water have received a considerable amount of attention due to their importance in basic solvation phenomena and their activity in biological systems such as the central nervous system.[110] The $Na^+ \cdot H_2O$ complex was first studied using photoionization efficiency measurements which yielded the intermolecular stretching frequency.[111] Recently, Rodham and Blake[112] obtained single-photon ZEKE spectra of this important complex and its deuterated analogue. The spectra, which are reproduced in Figure 17, provide improved ionization energies and frequencies of the intermolecular stretching vibrations (300 ± 5 cm^{-1} for $Na^+ \cdot H_2O$ and 295 ± 5 cm^{-1} for $Na^+ \cdot D_2O$). Up to three quanta of this vibration were observed in the ZEKE spectra, indicating that while the intermolecular bond length contracts upon ionization due to the introduction of the ion−dipole interaction, the change in bond length is not extreme. Both the neutral and cationic ground states of $Na \cdot H_2O$ are thought to adopt C_{2v} symmetry structures, which explains the absence of bending vibrations in the spectra.

One of the interesting aspects of the spectra present in the ZEKE study was that the vibrational features revealed partially resolved rotational struc-

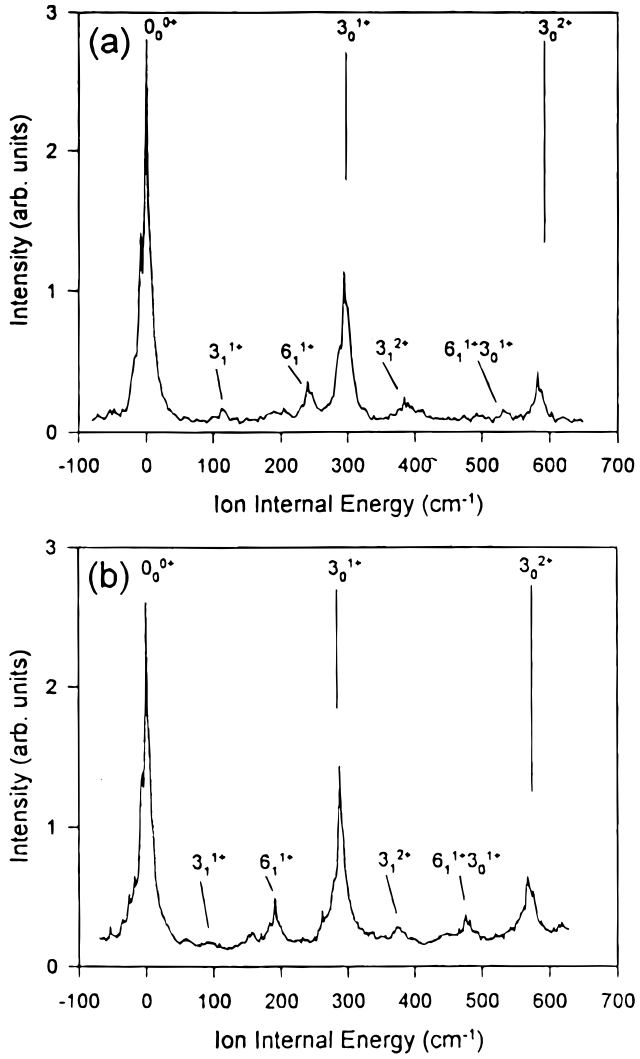

Figure 17. Single-photon ZEKE spectra of (a) Na·H_2O and (b) Na·D_2O. The intermolecular stretch progression is labeled 3_on^+. Other vibrational features were assigned to hot-band transitions. (Reprinted with permission from ref 112. Copyright 1997.)

ture. This prompted a new study where the spectra were reacquired with improved spectral resolution and the band profiles compared with rotationally resolved ab initio calculations.[113] The calculated spectra were found to agree well with the experimental spectra when the nonatomic-like behavior of the photoionization was included in the calculations. The rotational simulations are consistent with a bond contraction of 2% (i.e., 2.36−2.32 Å) upon ionization.

B. Complexes Containing Aromatic Molecules

i. Rare-Gas–Aromatic Complexes

Vibrationally resolved spectra of vdW complexes such as aromatic rare-gas complexes provide important benchmarks for understanding intermolecular forces.[114−119] The neutral benzene·Ar complex, which can be considered a prototype system, has been found to adopt a structure where the argon atom is bound 3.58 Å above the center of the benzene ring.[120] When one of the aromatic hydrogen atoms is replaced by a different functional group, the C_{6v} symmetry of the complex is reduced and the rare-gas atom may be displaced from the center of the aromatic ring. A number of aromatic−rare-gas atom complexes have been investigated using ZEKE spectroscopy. In general, the spectra display only modest vibrational structure indicating that there is little structural rearrangement upon ionization. Examples of recent work in this area include studies by Brutschy and co-workers on chlorobenzene·Ar, fluorobenzene·Ar_n (n = 1, 3), and *p*-difluorobenzene·Ar,[121,122] by Knee and co-workers on fluorene·Ar_n (n = 1−6) and 9-phenylfluorene·Ar_n (n = 1−4),[89,123] by Even and co-workers on perylene·rare-gas clusters,[124] and by Kimura and co-workers on azulene·Ar and toluene·Ar.[125,126] Several of these studies have provided information on vibrational predissociation in the S_1 state.

Despite the fact that aromatic−rare-gas complexes are well characterized in both the neutral and cationic ground states, high-level ab initio calculations on these systems are rather sparse with only benzene·Ar having been studied in detail previously.[127−129] Semiempirical methods have been employed to investigate the variation of the position adopted by the rare-gas atom upon substitution of the aromatic ring, and while the model predicted that the substituent should have only a small effect on the atom's position, it was noted that the method would have difficulties in modeling the phenol·Ar complex.[130] This system is of particular interest since the strongly hydrogen-bonding OH group may allow the argon atom to move into the aromatic plane and form a "hydrogen-bonding" structure.

A new ab initio study of the S_0 and D_0 states of phenol·Ar has predicted the existence of several stable isomeric structures (Figure 1 illustrates the two lowest energy neutral structures).[131,132] For the neutral cluster, the vdW isomer corresponded to the lowest energy neutral structure at all levels of theory. However, the corresponding cationic structure did not represent a stable structure using automatic (gradient) optimization techniques without counterpoise corrections. Calculations that did include counterpoise corrections suggest that this result is an artifact due to spin contamination of the wave function. Nonetheless, it is important to note that the hydrogen-bonded isomer is stable in both the neutral and cationic states and may therefore be observable in the REMPI spectrum.

These ab initio results have inspired a reinvestigation of the REMPI and ZEKE spectra of phenol·Ar to probe whether multiple isomers are present in the REMPI spectrum.[133] Bieske et al.[134] previously recorded the REMPI spectrum of phenol·Ar over the range 36300−36420 cm^{-1} and assigned the spectrum through comparison with structurally related complexes. A ZEKE spectrum was subsequently recorded via the $S_10°$ transition by Zhang and Knee[135] and appears to be consistent with a vdW-type structure. However, the assignment of the REMPI spectrum was somewhat ambiguous since vibrational features corresponding to only one of the two possible intermolecular bending vibrations could be definitively identified. The new experimental study therefore aimed to fully assign the S_1 state spectrum by

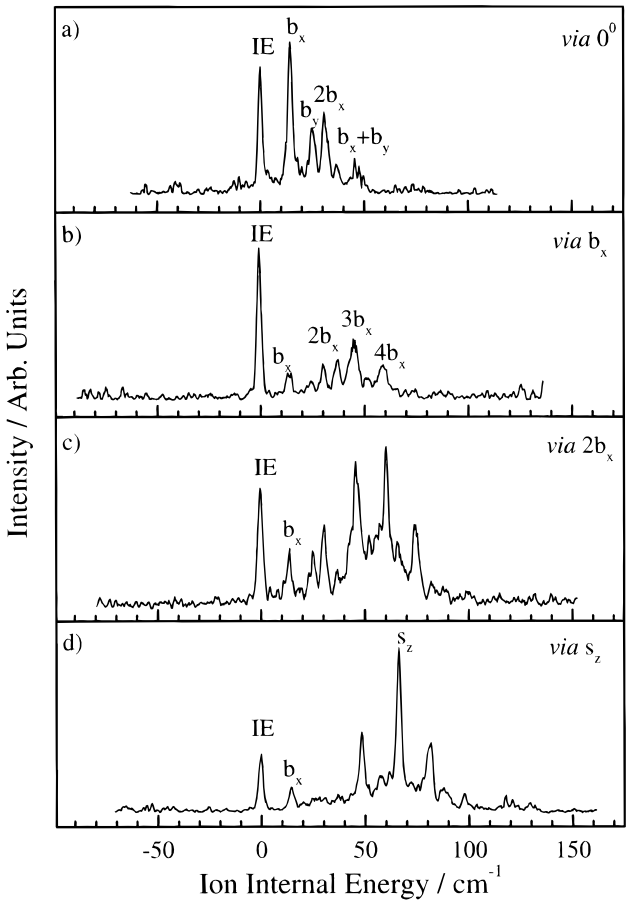

Figure 18. ZEKE spectra of phenol·Ar recorded via (a) $S_1 0°$, (b) $S_1 b_x$, (c) $S_1 2b_x$, and (d) $S_1 s_z$. Assignments of the vdW vibrational modes are included on the spectra. (Reprinted with permission from ref 133.)

obtaining ZEKE spectra via each spectral feature. If any of these features corresponds to the hydrogen-bonded isomer, excitation via that intermediate state should produce a distinctive ZEKE spectrum.

Figure 18 presents the ZEKE spectra of phenol·Ar recorded via four intermediate levels of the S_1 excited state of the neutral. All four spectra show vibrational progressions in the same three intermolecular modes (Figure 19), namely, the b_x bend (15 cm^{-1}), the b_y bend (25 cm^{-1}), and the s_z stretch (66 cm^{-1}), which are consistent with a vdW structure where the Ar atom binds above the aromatic ring. In addition, each spectrum displays the same ionization energy (68 452 $\pm$ 5 cm^{-1}). These observations indicate that there is no evidence of a significantly populated, hydrogen-bonding isomer of phenol·Ar present under the supersonic jet conditions employed. This is somewhat surprising in light of the ab initio predictions that this isomer should be stable in both the neutral and cation. One explanation is that the hydrogen-bonding isomer is unstable in the S_1 state, although this is unlikely since the dipole moment of phenol increases upon S_1-S_0 excitation.[136] The most probable explanation is that the system is quenched into the lowest energy, vdW isomer during the jet expansion. The population of different isomers in a molecular beam is a function not only of the relative energies of the isomers, but of the barrier height for interconversion of the isomers as well as the kinetic rates for

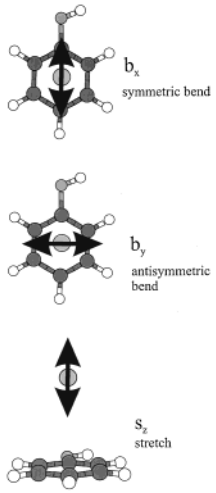

Figure 19. vdW normal modes of the phenol·Ar complex. (Reprinted with permission from ref 132.)

formation of competing isomers. It seems, therefore, that the barrier for interconversion of the hydrogen-bonding isomer to the vdW isomer is relatively modest.

Finally, to illustrate the complementary nature of ZEKE spectroscopy and IR−UV double-resonance techniques, we review some recent results by Piest et al. on aniline·Ar.[81] This cluster was studied several years ago by Knee and co-workers using ZEKE spectroscopy.[137] The ZEKE spectrum of [aniline·Ar]$^+$ displayed a harmonic vibrational progression spaced by 15 cm^{-1} built off the ionization energy feature which was assigned to the b_x intermolecular bend. However, as is typically the case for aromatic−rare-gas complexes, little vibrational structure was observed above the origin region due to weak Franck−Condon intensity, so that the cation's spectrum is rather incompletely characterized using this method alone. Piest et al. obtained IR spectra of aniline·Ar in both the S_0 and D_0 states using IR−UV double-resonance techniques. The spectra were acquired over the range 350−1700 cm^{-1} using a free-electron laser and therefore characterize the intramolecular vibrational frequencies of the complex. Figure 20 displays the IR absorption spectrum of the cationic complex. The observed frequencies appeared to be in good agreement with ab initio calculations conducted at the B3LYP/D95(d,p) level of theory which predict C_s and C_{2v} structures for the neutral and cationic complexes, respectively.

ii. Inorganic Ligand–Aromatic Complexes

A great number of spectroscopic studies of vdW complexes have involved systems solvated by rare-gas atoms, where the dominant interaction is usually dispersion. Molecular vdW complexes involving simple solvent ligands (e.g., N_2 and CO) have been studied less frequently[138] but are particularly interesting compared to the noble-gas atoms since they display similar polarizabilities[139] but can also interact via their quadrupole and dipole moments. The non-spherical symmetry of these ligands suggests the possibility of more geometrical conformations than for complexes solvated by an atom. Furthermore, these systems provide a bridge between aromatic·

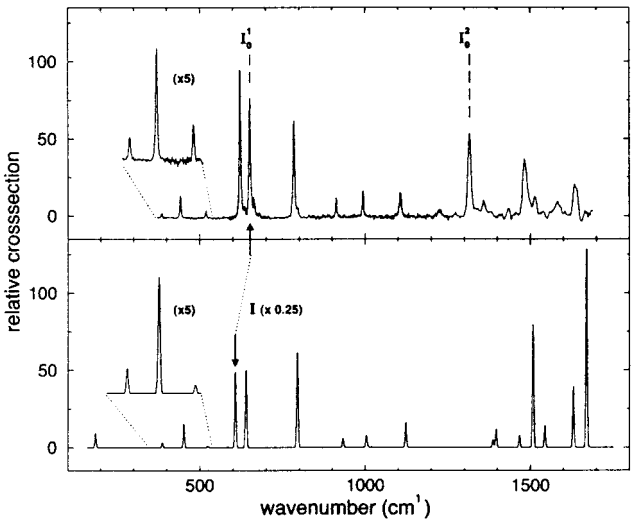

Figure 20. Upper trace: IR absorption spectrum of the aniline·Ar cation. The inversion mode (*I*) and its overtone are assigned on the spectrum. Lower trace: Calculated IR absorption spectrum of the aniline cation (C_{2v}). The inversion mode is not calculated correctly and the spectrum has therefore been scaled by a factor of 4. (Reprinted with permission from ref 81. Copyright 1999.)

noble-gas and hydrogen-bonded aromatic·H_2O complexes such as phenol·H_2O.[52,140,141]

Benzene·N_2 represents one of the simplest complexes of an aromatic molecule with a diatomic ligand. Nowak et al. used REMPI spectroscopy to study Benzene·N_2 and concluded that the N_2 rotates freely around the Benzene−N_2 intermolecular bond axis in the S_0 state, while the rotational barrier is 20 cm^{-1} in the S_1 state.[142] Weber et al. subsequently obtained a high-resolution REMPI spectrum of the complex which indicated that N_2 is located parallel to the benzene ring at a distance of 3.5 Å in the S_1 state but rotates freely around the bond axis.[143] Kimura and co-workers recently published a ZEKE spectrum of the complex which was the first of an aromatic molecule with a diatomic ligand.[144] The cation origin band was broad (fwhm ∼ 50 cm^{-1}), showing low-frequency spacings of 6 cm^{-1}, which these authors assigned to progressions of the vdW bending and torsion modes.

The phenol·N_2 and phenol·CO complexes provide examples of systems which can form many more isomers than a benzene·RG complex.[145] Two main binding sites to the phenol moiety can be anticipated: above the center of the aromatic ring or at the hydroxyl group. Some of the stable isomers of the neutral phenol·N_2 complex obtained from ab initio calculations are illustrated in Figure 21. Note that for each isomer of phenol·N_2, there are two possible isomers of phenol·CO corresponding to either the carbon or oxygen atom of CO binding to the phenol molecule. Only the hydrogen-bonded isomers were found to be stable in the cationic ground state, indicating that ZEKE spectra of phenol·N_2 and phenol·CO should correspond to structures where the ligand binds at the hydroxyl group.

The results of this ab initio study were provocative in view of several ZEKE spectra of aromatic−N_2/CO complexes (e.g., aniline·N_2, aniline·CO, fluorobenzene·

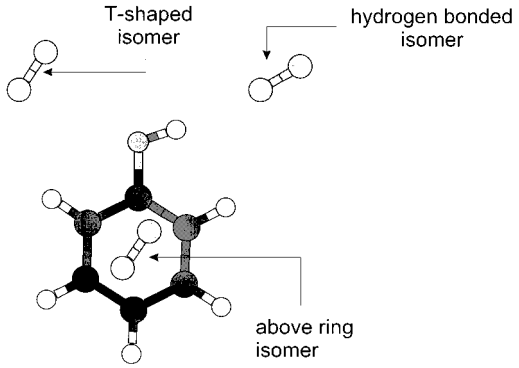

Figure 21. Possible isomers of the neutral phenol·N_2 complex, identified from ab initio calculations at the RHF/6-31G* level of theory. (Reprinted with permission from ref 145. Copyright 1999.)

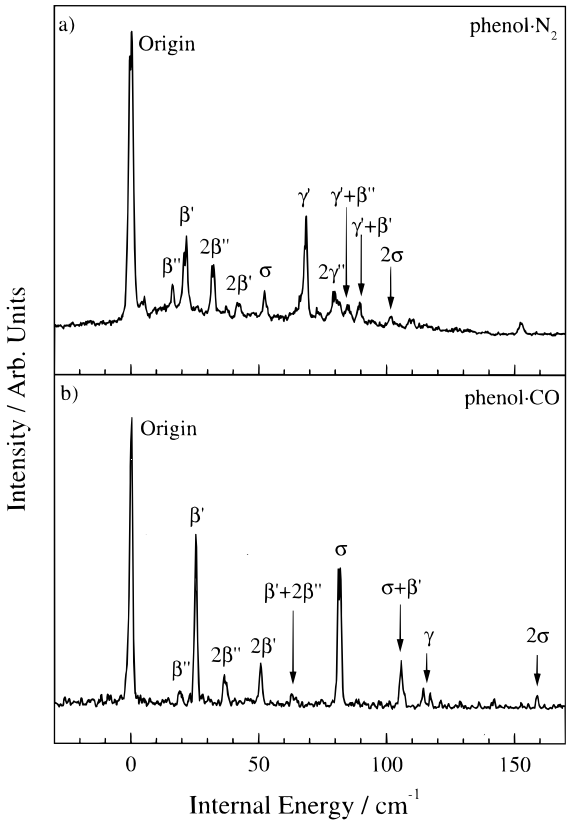

Figure 22. Two color (1+1′) REMPI spectra of (a) phenol·N_2 and (b) phenol·CO. Assignments of vdW vibrational modes are included on the spectra. Note that these modes appear at higher frequency for the more strongly bound phenol·CO complex. (Reprinted with permission from refs 31 and 67. Copyright 1998 and 1999.)

N_2) which appear to correspond to structures where the ligand binds above the aromatic ring.[145,146,147] Figure 22 shows the (1 + 1′) REMPI spectra of phenol·N_2 and phenol·CO.[26] Both spectra display relatively extensive excitation of low-frequency vdW vibrational modes, unlike the REMPI spectra of aromatic rare-gas complexes where the ligand binds above the aromatic ring. These vibrational features were tentatively assigned to excitation of the in-plane bend (β'), in-plane wag (γ'), and intermolecular stretch (σ) modes illustrated in Figure 23. (For the C_s symmetry structures indicated by the calculations, the intermolecular normal coordinates are classified

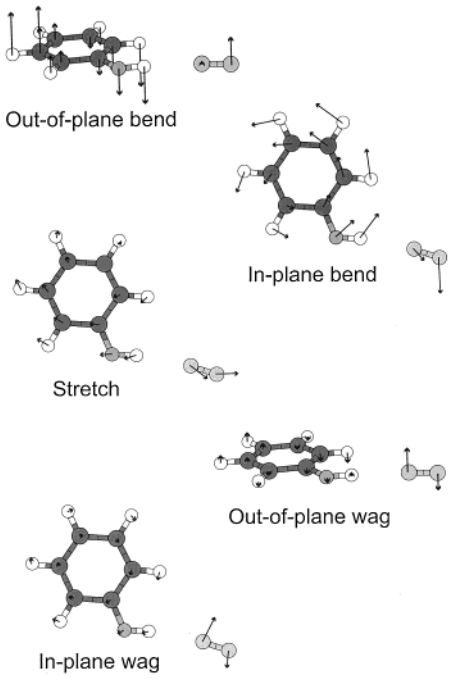

Figure 23. vdW modes of the hydrogen-bonding phenol·N_2/CO complexes. (Reprinted with permission from ref 132.)

according to whether they transform as a′ or a″, and only a′ modes should be observed in single quanta.)

A number of ZEKE spectra were recorded for each complex via different intermediate levels of the S_1 state to confirm the assignment of the vibrational features in the REMPI spectra. For both complexes, extensive vibrational progressions were observed (ion internal energy > 1000 cm^{-1}) which were assigned to excitation of the same intermolecular vibrational modes (β', γ', and σ) by comparison with harmonic frequencies obtained from the ab initio calculations.[145] Table 1 compares the experimental and ab initio frequencies for phenol·N_2 and phenol·CO. The extensive vibrational excitation observed in the ZEKE spectra of these complexes indicates that a substantial geometry change occurs upon ionization and contrasts dramatically with the rather limited vibrational excitation which was observed in the ZEKE spectra of aniline·N_2, aniline·CO, and fluorobenzene·N_2.[144,146]

The spectral shifts observed in both the REMPI and ZEKE spectra provide a good indication of the changes in binding energy that occur following excitation from the neutral ground state to the S_1 and D_0 states. Generally, the larger the red shift, the stronger the interaction between the phenol molecule and the ligand. Table 2 lists the red shifts for phenol·N_2 and phenol·CO, along with the values for phenol·Ar and phenol·H_2O for comparison.[134,135,148] For both the S_1-S_0 and S_1-D_0 red shifts, the values for phenol·N_2 and phenol·CO lie between those of phenol·Ar and phenol·H_2O. This suggests that the intermolecular bonds in the phenol·N_2/CO complexes are of intermediate strength relative to the vdW bond in phenol·Ar and the hydrogen bond in phenol·H_2O. Clearly, the position at which the ligand binds to the phenol moiety also has an important influence on the magnitude of the red shift. In $C_6H_5-X\cdot N_2$ (X = F, Cl, Br) complexes, where the nitrogen molecule is thought to lie above the aromatic ring,[149] the S_1-S_0 red shifts are close to that of the similarly structured phenol·Ar cluster (14, 19, and 22 cm^{-1}, respectively). Thus, the observed red shift for phenol·N_2 supports the structure proposed above where the nitrogen binds directly to the OH group.

Table 2. Comparison of Spectral Red Shifts (in cm^{-1}) for Phenol·X (X = Ar, N_2, CO and H_2O) Complexes Compared to Phenol

transition	phenol·Ar	phenol·N_2	phenol·CO	phenol·H_2O
S_1-S_0	33	100	190	353
D_0-S_0	171	1205	1766	4602

MATI dissociation spectra were recorded to obtain accurate binding energies for the cationic complexes. Figure 24 displays the MATI spectra, recorded via the respective S_1 intermediate states, over the spectra region from the ionization energy through the dissociation threshold with the inserts presenting expanded views of the threshold region. The cationic binding energies can be combined with the adiabatic ionization energies and S_1-S_0 red shifts to obtain accurate binding energies for the S_0 and S_1 states. Table 3 lists the values obtained along with the corresponding binding energies for phenol·Ar. Several points should be noted. For both phenol·N_2 and phenol·CO, the binding energies increase substantially upon ionization due to the introduction of the charge−quadrupole interaction. The increased binding energy will be accompanied by a decrease in the intermolecular bond length, which is evident in the extensive excitation of σ in the ZEKE spectra. Second, the binding energies of phenol·N_2 and phenol·CO in each of the electronic states are considerably larger than the values for the vdW-bound phenol·Ar complex.[50]

It is also of interest to directly compare the binding energies of phenol·N_2 with those of phenol·CO. Table 3 illustrates that the binding energies of phenol·CO in all electronic states increase substantially compared to phenol·N_2. While ab initio calculations

Table 1. Experimental Intermolecular Vibrational Frequencies of $[Phenol\cdot N_2]^+$ and $[Phenol\cdot CO]^+$ Compared to the ab Initio Harmonic Frequencies of the Hydrogen-Bonded Isomers of the Cationic Complexes Calculated at the UMP2/6-31G* Level of Theory

		$[phenol\cdot N_2]^+$		$[phenol\cdot CO]^+$	
mode symbol	description of motion	exp (cm^{-1})	calcd (cm^{-1})	exp (cm^{-1})	calcd (cm^{-1})
β''	out-of-plane bend		35		41
β'	in-plane bend	35	38	42	46
σ	stretch	117	118	130	136
γ''	out-of-plane wag		127		162
γ'	in-plane wag	130	132	160	168

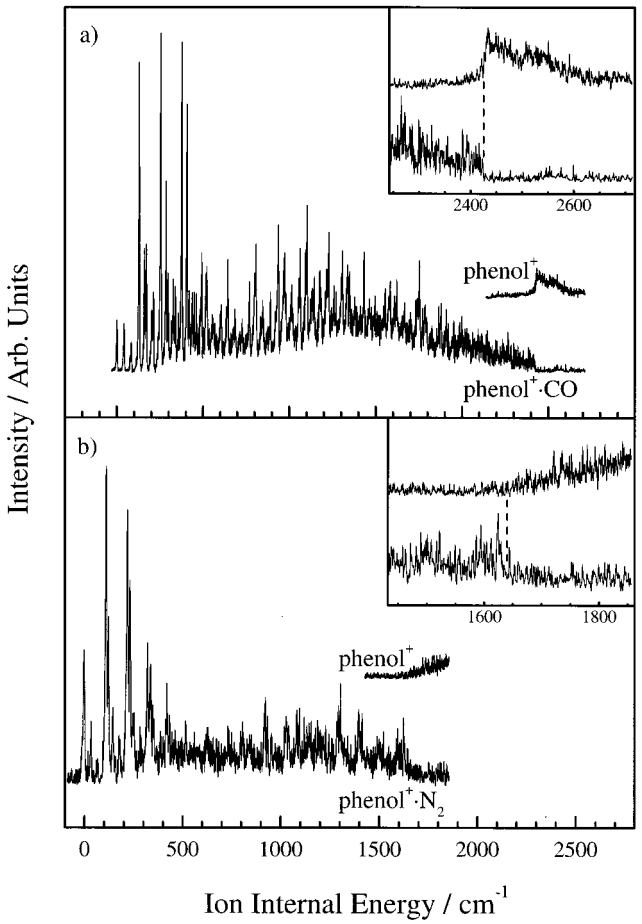

Figure 24. MATI dissociation spectra of (a) phenol·N_2 and (b) phenol·CO recorded via the $S_1 0°$ band origins. The inserts show expanded plots of the dissociation region with the dashed lines indicating the position of the field-free ionic dissociation thresholds. (Reprinted with permission from ref 67. Copyright 1999.)

Table 3. Comparison of Binding Energies (in cm^{-1}) for the Phenol·X (X = Ar, N_2 and CO) Complexes

state	phenol·Ar	phenol·N_2	phenol·CO
S_0	364 ± 13	435 ± 20	659 ± 20
S_1	397 ± 13	535 ± 20	849 ± 20
D_0	535 ± 3	1640 ± 10	2425 ± 10

provide a complete theoretical description of the intermolecular bond, it is useful to develop a more chemically intuitive picture of intermolecular bonding by assessing the contributions of the various classical electrostatic interaction terms to the binding energy. The interaction energies will be composed of a number of terms including polarization, dispersion, repulsion, phenol dipole−ligand quadrupole, and, for the cation, ion−quadrupole. Since the polarizabilities of CO and N_2 are very similar,[139] most of these terms will be similar for both complexes with the exception of the quadrupole interactions as the quadrupole moment of CO is approximately twice that of N_2.[150] Therefore, the differences between the binding energies of the two complexes in each of the electronic states can mainly be attributed to the difference in the phenol−quadrupole interactions. The binding energies increase by approximately 50% as the quadrupole moment of the ligand doubles, leading to the conclusion that while quadrupole terms contribute approximately one-half of the interaction energy in phenol·N_2, they contribute closer to two-thirds of the interaction energy in phenol·CO. It would be useful to test this idea in future studies of the interaction energies of other small ligands with phenol (e.g., NO, O_2).

Braun et al.[151] also investigated the transition from vdW to hydrogen bonding by MATI dissociation spectroscopy of complexes of indole with argon, water, and benzene. The experiment demonstrated the vdW character of the indole·Ar complex and the hydrogen-bonding character of the indole·H_2O complex. Indole·benzene was also found to possess a hydrogen bond since it displayed comparable binding energies in the neutral (1823 cm^{-1}) and ionic (4581 cm^{-1}) ground states to the indole·H_2O complex (1632 and 4790 cm^{-1}, respectively).

To summarize, the REMPI, ZEKE, and MATI dissociation spectra of phenol·N_2 and phenol·CO appear consistent with structures where the ligand binds to the hydroxyl group of the phenol molecule. For both systems, there was no evidence of other isomers present under the molecular beam conditions employed. Following this work, Mikami and coworkers[80] used IRIDS and infrared photodissociation spectroscopy to directly probe the structure of phenol·N_2 by investigating whether the phenol OH stretching frequency is perturbed in the neutral and cationic states of the complex. The experiment revealed that the frequency of the stretch was indeed red-shifting compared to phenol (−5 and −159 cm^{-1} for the S_0 and D_0 states, respectively) in line with a hydroxyl-bound structure. The work described above therefore represents the first report of N_2/CO solvated aromatic complexes where the ligand is not bound to the π-system of the benzene ring.

C. Aromatic Hydrogen-Bonding Complexes

i. Conformational Isomerism

Molecular conformation plays a crucial role in selectivity and function of biologically active molecules, such as neurotransmitters and enzymes. Hydrogen-bonded interactions, both within molecules and with adjacent solvent molecules, are ubiquitous in determining conformation.[58,152−158] Simons and coworkers investigated the conformational preferences of a series of flexible organic molecules and their hydrated complexes, many of which are model systems for simple biological molecules, using a combination of REMPI techniques and partially rotationally resolved band contour analysis.[58,152−154] Ab initio-calculated rotational constants have been used to simulate rotational band contours to aid the rotational assignments. The strategy of conformational assignment has been made even more powerful by the discovery of a correlation between the polarization of the $\pi-\pi^*$ electronic transitions in the aromatic chromophore and the conformational structures adopted by the side chain,[155] which can be further modulated by their interaction with bound water molecules.

As a specific example, we consider the hydrated *p*-tyrosol (4-hydroxy phenyl ethanol) system.[152] For

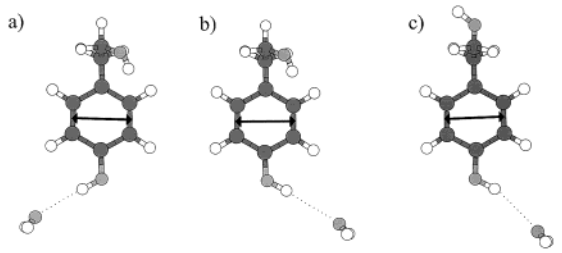

Figure 25. Schematic conformational structures of *p*-tyrosol·H_2O illustrating (a) trans gauche, (b) cis gauche, and (c) anti conformations. (Reprinted with permission from ref 152. Copyright 1999.)

the monomer, the spectra reveal that a strong preference exists for a folded gauche conformation of the flexible side chain, which is stabilized by a hydrogen-bonding interaction between the alcoholic OH group and the aromatic ring. Folded conformations that do not allow this hydrogen-bonding interaction were not observed experimentally. UV hole burning of the REMPI spectrum identified a number of additional conformational isomers, which were assigned as gauche-cis, gauche-trans, and extended anti conformers. In the hydrated complex, the water ligand preferentially binds to the phenolic OH rather than the alcoholic OH group.[152] (A similar binding preference has been observed in a ZEKE study of the phenol·ethanol complex[159]). The tagging of the phenolic group by the hydrogen-bonding water molecule allows the unambiguous assignment of the cis- and trans-gauche conformers (Figure 25) through rotational band contour analysis. The partially resolved spectra in this study were acquired using LIF. However, it should be emphasized that the lower resolution REMPI precursor spectra are essential in assigning spectra to the correct cluster.

ii. IR–UV Double-Resonance Spectroscopy

Over the last 5 years, a large number of studies of both neutral and cationic water clusters have been facilitated by the application of IR−UV double-resonance spectroscopy.[28−30,78−80,160−166] In this section we consider three examples from the groups of Kleinermanns, Zwier, and Brutschy.

Kleinermanns and co-workers conducted a number of studies on phenol−water clusters which are prototypes for hydrogen-bonding aromatic systems.[79,163] It should be noted that clusters larger than phenol·$(H_2O)_2$ are not amenable to study using ZEKE spectroscopy since large geometry changes occur upon ionization, leading to negligible Franck−Condon factors over the threshold region. Recently, phenol·$(H_2O)_7$ and phenol·$(H_2O)_8$ have been investigated in both the neutral and cationic ground states using IR−UV double resonance.[79,163] For the neutral system, two isomers of phenol·$(H_2O)_7$ and three isomers of phenol·$(H_2O)_8$ were distinguished in the REMPI spectra by UV hole burning (Figure 26) and their IR spectra recorded. All of the IR spectra contain four characteristic groups of OH stretching vibrations which give insight into the hydrogen-bonding network. Ab initio calculations show that the minimum energy structures for phenol·$(H_2O)_{7,8}$ are very similar to the corresponding water clusters which are based on regular $(H_2O)_8$ cubes. The calculations indicate that for phenol·$(H_2O)_8$, the phenol can attach to and insert itself in the water network. For the cationic clusters, comparison of the IR spectra with ab initio calculations indicate that the second and third solvation shells are at least partially filled and proton transfer occurs within the phenol·$(H_2O)_{7,8}^+$ clusters on the nanosecond time scale of the experiment. This method is especially suited to studies of ions that undergo large structural changes (e.g., proton-transfer reactions) after resonant ionization. Furthermore, the approach will facilitate time-resolved measurements of ionic chemical reactions.

Zwier and co-workers employed IR−UV double resonance, which they have termed RIDIR spectroscopy, to characterize the structure of neutral water and, more recently, methanol clusters with benzene.[28,160−162] This work builds off earlier REMPI studies of systems such as benzene·H_2O.[167] As in the work of the Kleinermanns' group discussed above, cluster structures are assigned by comparing the IR spectra with ab initio (density functional theory) calculations. The benzene·$(H_2O)_8$ system has been characterized as adopting a "molecular ice cube" structure where the water molecules form a cube above the aromatic ring.[28] This work has recently been discussed in another review.[5] Unlike the water clusters, the solvent forms linear chains for the n = 1−3 clusters whereas the larger clusters again adopt cyclic geometries in the benzene·$(methanol)_n$ (n = 1−6) clusters.[160,161]

Most recently, mixed benzene·$(H_2O)_n$·$(CH_3OH)_m$ ($n + m \leq 4$) clusters (referred to as BW_nM_m in the following) have been investigated to bridge between the pure water and methanol clusters studied previously.[78] These experiments address the issue of preferential solvation. Both benzene and water are highly soluble in methanol but immiscible in one another, so that studies of their clusters probes the structural consequences of this disruption on a molecular scale. For $n + m = 2$, a single BWM isomer is observed corresponding to a structure where methanol accepts a hydrogen bond from water and forms a π hydrogen bond with benzene. The $n + m = 3$ results reveal the subtle effects that solvent composition can have on the lowest energy structure of the cluster, since two isomers of BW_2M are observed but just one BWM_2. Both BW_2M isomers possess transitions characteristic of cyclic W_2M subclusters in which water is π-hydrogen bonded to benzene but differ in the position of the methanol in the hydrogen-bonded rings. However, the WM_2 unit within the BWM_2 cluster adopts a chain geometry, with the water molecule being most distant from the aromatic ring. All members of the $n + m = 4$ series possess cyclic W_2M_2 subclusters in which one of the free OH groups on a water molecule in the cycle is used to π-hydrogen bond to benzene. Figure 27 displays an overview of RIDIR spectra for the $n + m = 4$ systems illustrating this point.

While the π-hydrogen bonds evident in the benzene·$(solvent)_n$ clusters studied by Zwier and co-workers[28,78,160−162] and in the flexible aromatic systems investigated by Simons and co-workers[58,152−154]

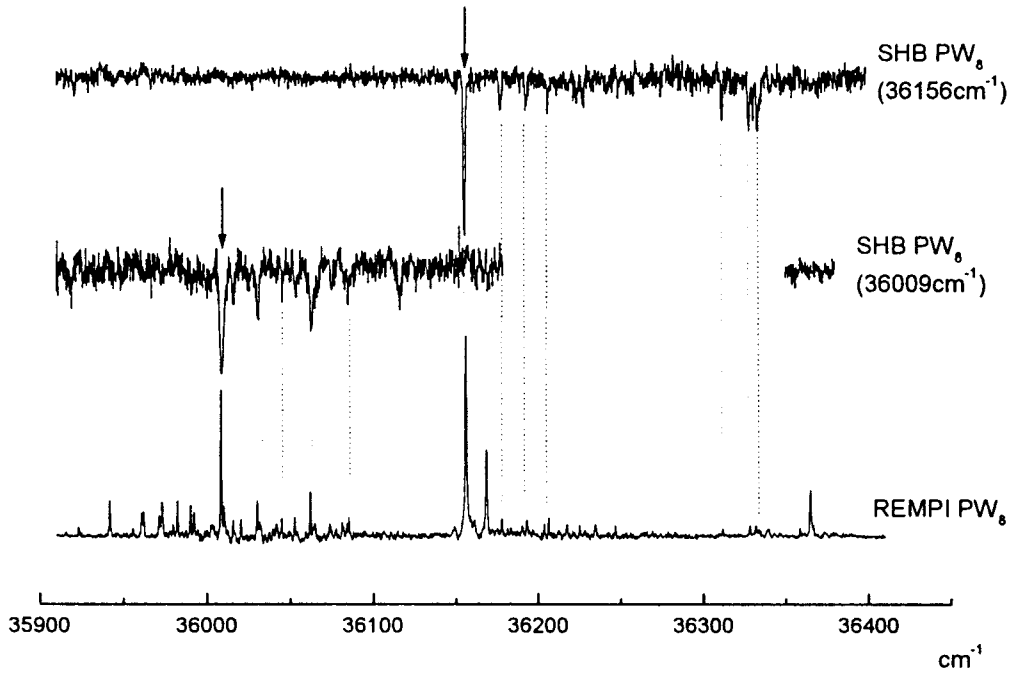

Figure 26. UV hole-burning spectra of two phenol·$(H_2O)_8$ isomers. The REMPI spectrum is shown for comparison and illustrates that three isomers are present. (Reprinted with permission from ref 163. Copyright 1999.)

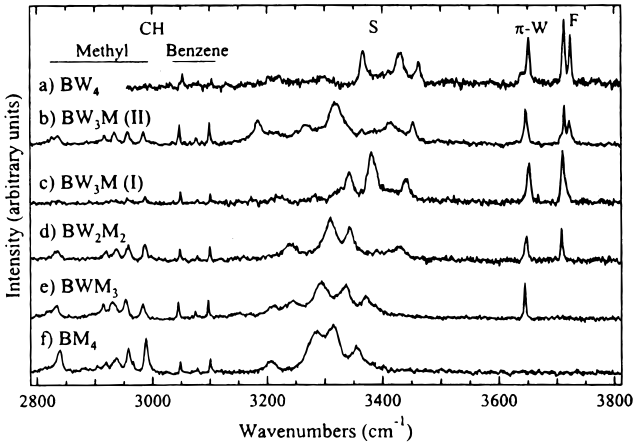

Figure 27. RIDIR spectra of benzene·H_2O_n·methanol$_m$ clusters with $n + m = 4$. Characteristic absorptions due to free OH stretch (3710−3730 cm^{-1}), π hydrogen-bonded OH stretch (∼3650 cm^{-1}), single donor OH stretch (3150−3500 cm^{-1}), benzene CH stretch (3050−3100 cm^{-1}), and methyl CH stretch (2800−3000 cm^{-1}) are apparent. All clusters, except benzene·methanol$_4$, are complexes to benzene through a water−π hydrogen bond. (Reprinted with permission from ref 78. Copyright 1999 American Chemcial Society.)

are well-known, little is understood about how the aromatic chromophore influences the spectral shift of its absorption band. This issue has been addressed by Brutschy and co-workers,[29] who have acquired the IR spectra of a series of substituted benzene·$(H_2O)_{1-4}$ complexes over the region of the ν_1 symmetric and ν_3 antisymmetric OH stretching vibrations using IR−UV double-resonance spectroscopy. Water clusters with *p*-difluorobenzene, fluorobenzene, benzene, toluene, *p*-xylene, and anisole were investigated. As in the water clusters studied by Gruenloh et al.,[28] the water molecules attach as subclusters to the chromophores, except for anisole·$(H_2O)_{1,2}$, where the waters form ordinary hydrogen bonds to the oxygen of the methoxy group. For the other complexes, a π-hydrogen bond is formed between one of the free OH groups of a water subcluster and the π system of the chromophore. Depending on the strength of this interaction, the frequency of the respective absorption band exhibits a characteristic red shift which can be related to the total atomic charges on the aromatic ring. The more electron donating the substituent, the more pronounced is the red shift observed, with the red shift being a linear function of the ab initio-calculated total charge on the benzene ring. These results illustrate the importance of the electrostatic interaction in the π-OH hydrogen bond.

iii. Excited-State Dynamics of Phenol·$(NH_3)_n$ Clusters

Proton transfer is an important chemical and biological process, and a number of gas-phase studies have been performed to characterize the process in hydrogen-bonding clusters.[91−95] Excited-state proton transfer can be investigated using time-resolved REMPI techniques, which provide information on the potential-energy surface of the reaction in addition to kinetic data. For example, the position of barriers on the reactive surface can be probed by monitoring the appearance of specific products. Bernstein and co-workers used these methods to study naphthol·$(NH_3)_n$ clusters,[168] and Castleman and co-workers recently investigated the 7-azaindole dimer,[94] while additional studies have been conducted by the groups of Syage and Zewail.[91−92]

Despite the plethora of experiments which have been performed in this area, recent work by Jouvet and co-workers illustrated that some care is necessary in interpreting the results of these pump−probe experiments.[93] Small phenol·$(NH_3)_n$ clusters were studied using two-color two-photon and one-photon VUV ionization to disentangle the contributions of various dissociation or reaction paths in the excited and ionic states. In the two-color experiments, $(NH_4)^+$-

$(NH_3)_{n=1,5}$ fragments are observed with large delays (up to several hundred nanoseconds) between the pump and probe lasers, whereas the same fragments were not observed using one-color VUV ionization. These results were explained by invoking a new deactivation channel in the excited state where a *hydrogen atom* is transferred, i.e., $PhOH{\cdot}(NH_3)_n \rightarrow 6PhO{\cdot} + (NH_4)(NH_3)_{n-1}$. The delayed $(NH_4)^+(NH_3)_n$ fragments then correspond to direct ionization of the $(NH_4)(NH_3)_{n-1}$ clusters produced in the excited state. This experiment illustrated that earlier interpretations of the experimental data (i.e., proton transfer in the S_1 state) were in fact incorrect.

iv. Influence of Secondary Functional Groups on a Hydrogen Bond

The preference of a solvent molecule for certain binding sites on a solute molecule is a problem of general chemical interest. In the low-temperature environment of a free jet expansion, isomeric molecular complexes can be generated with a single solvent molecule 'frozen' at different binding sites on the solute when the barrier for interconversion between isomers is sufficiently high. An example is provided by dihydroxybenzenes, which can exist in different isomeric forms that are related through rotations of the OH groups.[169−172]

REMPI and ZEKE spectroscopy were combined in a recent study of resorcinol·H_2O (1,3-dihydroxybenzene·H_2O) clusters which explored different binding sites which occur in rotational isomers of the complex.[60] In the related phenol·H_2O complex, which has been extensively studied as a prototype for

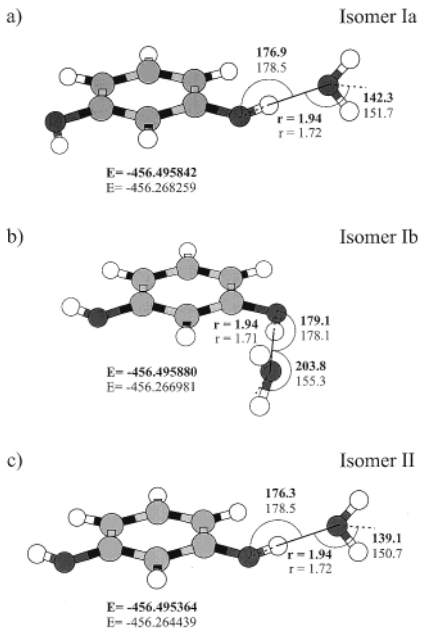

Figure 28. Geometrical structures and energies of the resorcinol·H_2O isomers. Numbers in bold refer to the neutral complexes calculated at the RHF/cc-pVDZ level, while numbers in plain text refer to the cationic complexes calculated at the UHF/cc-pVDZ level. Energies are given in hartrees, molecular bond lengths in angstroms, and angles in degrees. The dihedral angle between the H_2O and phenyl plane is 90.0° in all of the complexes. (Reprinted with permission from ref 60. Copyright 1999 American Chemical Society.)

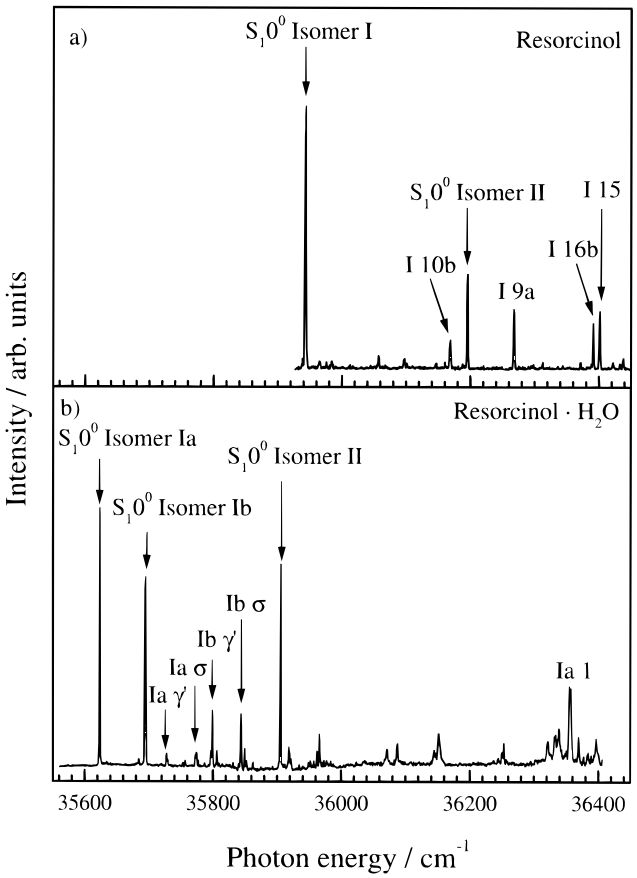

Figure 29. Two-color (1+1′) REMPI spectra of (a) the resorcinol monomer and (b) resorcinol·H_2O recorded with the ionizing photon set to 30 800 cm^{-1}. Assignments of the in-plane wag (γ') and stretch (σ) intermolecular vibrations are included in Figure 29b. (Reprinted with permission from ref 60. Copyright 1999 American Chemical Society.)

hydrogen-bonding interactions,[14,148,173] the water molecule binds as an acceptor to the phenol OH group. Ab initio calculations (HF/cc-pVDZ) predicted that this primary interaction also dominated intermolecular binding in resorcinol·H_2O with the isomeric complexes pictured in Figure 28 representing the three lowest energy minima. It is notable that the solvent adopts a 'localized' binding site in these structures rather than binding along the dipole moment of the solute. The prediction of multiple isomers was interesting since it suggested that the extent to which the intermolecular hydrogen bond is perturbed by a secondary functional group can be investigated by acquiring spectra of the various isomers.

Spectral hole burning of the resorcinol·H_2O REMPI (Figure 29) spectrum revealed the presence of three rotational isomers, with S_1 origins at 35 624 ± 1, 35 695 ± 1, and 35 905 ± 1 cm^{-1}. The $S_1 0°$ transitions were assigned to resorcinol·H_2O isomers Ia, Ib, and II (Figure 28) by comparing the $S_1 0°$ transition in phenol·H_2O with the position of the $S_1 0°$ transitions of the resorcinol monomers. *Note that this allows the resorcinol·H_2O isomer I complexes to be distinguished from isomer II.* The S_1-S_0 red shifts (320, 249, and 291 cm^{-1}, respectively) are all smaller than the red shift observed for phenol·H_2O (353 cm^{-1}), indicating that water binds less strongly to resorcinol than to

Table 4. Ab Initio Harmonic Frequencies (in cm^{-1}) of the Intermolecular Vibrations of the Rotational Isomers of [Resorcinol·H_2O]$^+$ at the UHF/cc-pVDZ Level of Theory. Experimental Frequencies Are Displayed in Parentheses

mode	isomer Ia	isomer Ib	isomer II
β''	59.8	69.4 (63[a])	59.0
β'	91.4	79.8 (71)	90.8
τ	179.3	167.1	179.2
σ	209.7 (215)	216.1 (223)	208.7 (214)
γ'	366.8 (369)	341.8 (311)	370.8 (370)
γ''	382.9	381.9	383.2

[a] Calculated from $2\beta''$.

phenol. Intermolecular vibrational modes observed in the REMPI spectra also appear at lower frequencies than in phenol·H_2O.[60,148] For example, the intermolecular stretch appears at 150 and 148 cm^{-1} in isomers Ia and Ib of resorcinol·H_2O, respectively, but at 157 cm^{-1} in phenol·H_2O, with this pattern being replicated for the in-plane wag.

The ab initio calculations (Figure 28) revealed that for the neutral isomers Ia and II, the angles of the C_{2v} axis of the water molecule to the OH group (142.3° and 139.1°) are very similar to the angle of 141.2° found in phenol·H_2O. However, in neutral isomer Ib, this angle is considerably distorted (203.8°), presumably due to the hydrogen atoms of the water molecule being stabilized by an interaction with the second OH group of resorcinol. The calculations predicted that a substantial geometry change occurs along this coordinate between the S_0 and D_0 states for isomer Ib, with the effect that this angle is similar in the three cationic complexes. Therefore, while the ZEKE spectra of isomers Ia and II should be similar, the spectrum of isomer Ib should be distinctive. The similarity of structures Ia and II is reflected in the intermolecular frequencies displayed in Table 4, which suggest that these isomers should be difficult to assign on the basis of their ZEKE spectra alone.

Figure 30 displays the ZEKE spectra of the three resorcinol·H_2O isomers recorded via the respective $S_1 0°$ intermediate states. The lowest energy feature in each spectrum was assigned to the vibrational ground state of the cation, giving ionization energies of 62 635 ± 2, 62 771 ± 2, and 63 085 ± 3 cm^{-1} for isomers Ia, Ib, and II, respectively. The ionization energies correspond to red shifts of 4060 ± 4 (Ia), 3924 ± 4 (Ib), and 4063 ± 4 cm^{-1} (II) compared to the respective monomer transitions, all of which are considerably smaller than the ionization energy red shift of 4601 ± 8 cm^{-1} observed in the phenol·H_2O cluster.[148] The ZEKE spectra of each isomer display extensive vibrational features that can mainly be attributed to two modes, one displaying a progression spaced by ~220 cm^{-1} (the intermolecular stretch, σ) and the other by ~350 cm^{-1} (in-plane wag, γ'). Both the IE red shifts and the frequencies of the intermolecular modes indicate that the ligand is more weekly bound in [resorcinol·H_2O]$^+$ than in [phenol·H_2O]$^+$.

The ZEKE spectra were assigned to the three rotational isomers by comparing the experimental frequencies of the σ and γ' modes to the ab initio results. The assignment of isomer Ib was relatively straightforward since the γ' mode occurs at a substantially lower frequency compared to the other isomers. The vibrational constants of σ and γ' are relatively similar in isomers Ia and II, although σ appears at a slightly higher frequency while γ' occurs at a slightly lower frequency in isomer Ia compared to isomer II, leading to the assignment shown in Table 4. This assignment is strengthened by the argument based on the S_1-S_0 red shifts discussed above.

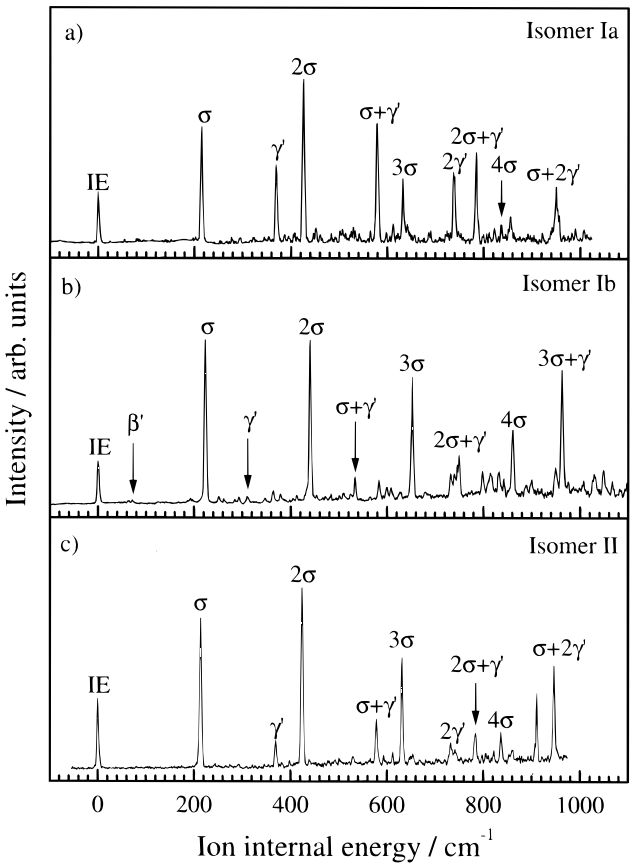

Figure 30. ZEKE spectra of resorcinol·H_2O recorded via the $S_1 0°$ state of (a) isomer Ia, (b) isomer Ib, and (c) isomer II. Each spectrum is displayed relative to the respective ionization energy. Assignments of the in-plane bend (β'), in-plane wag (γ'), and intermolecular stretch (σ) modes are included on the spectra. (Reprinted with permission from ref 60. Copyright 1999 American Chemical Society.)

If the spectra of the resorcinol·H_2O isomers are compared, the isomer Ib spectra deviate most from the other isomer spectra and from the spectra of phenol·H_2O. The ab initio results indicate that this effect originates from the considerable distortion of the water molecule-resorcinol OH group geometry from the optimal geometry for hydrogen bonding in the neutral cluster, possibly due to an interaction of the water molecule hydrogen atoms with the oxygen atom of the second OH group. This interaction may explain the blue shift of the $S_1 0°$ transition compared to the other resorcinol·H_2O isomers, since a similar interaction in the phenol dimer cluster results in a blue shift of the $S_1 0°$ transition compared to the phenol monomer.[174] The proximity of the second OH group to the hydrogen bond is also evident in the large $\omega_e x_e$ value of γ' observed for this isomer.[60]

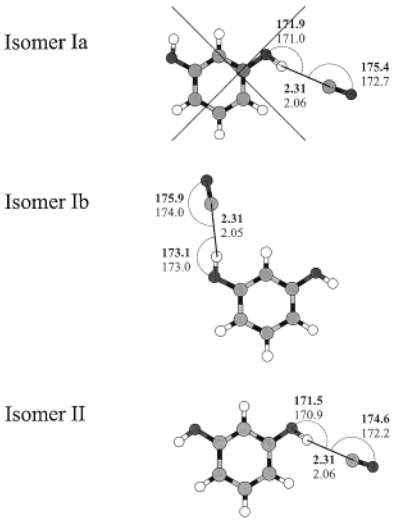

Figure 31. Geometrical structures of rotational isomers of resorcinol·CO. Numbers in bold refer to the neutral complexes calculated at the RHF/6-31G* level, while numbers in plain text refer to the cationic complexes calculated at the UHF/6-31G* level. Molecular bond lengths are given in angstroms and angles in degrees. The missing rotational isomer is crossed out. (Adapted with permission from ref 61.)

The ab initio geometries of the intermolecular bonds in isomers Ia and II are quite close to that of phenol·water, although in isomer Ia the water molecule tilts slightly away from the free OH group of resorcinol presumably due to a slightly repulsive interaction between one of the water hydrogens and the hydrogen of the free OH group. This situation is reversed in isomer II, where the water molecule tilts slightly toward the secondary OH group due to an interaction with the oxygen of the free OH group. This difference might explain the blue shift in the $S_1 0°$ transition of isomer II compared to isomer I and is again reflected in the comparably larger value of $\omega_e x_e$ for the γ' mode of isomer II.[60]

While this section of the review is mainly concerned with clusters of aromatic molecules with water, we will briefly discuss some related work on the resorcinol·CO cluster[61] since it highlights some interesting points. Ab initio calculations at the MP2/6-31G* level of theory predict the existence of three rotational isomers of resorcinol·CO (Figure 31) which are analogous to the rotational isomers of resorcinol·H_2O discussed above. [Note that as in phenol·CO, the CO molecule hydrogen bonds to resorcinol through its carbon atom (see section IV.B.ii).] However, spectral hole burning of the (1 + 1) REMPI spectrum of resorcinol·CO (Figure 8) indicated that only *two* rotational isomers were present.

It is currently unclear why only two resorcinol·CO rotational isomers are formed under the free jet expansion conditions employed in this study whereas three rotational isomers of resorcinol·H_2O were observed. This phenomenon presumably relates to the different barrier heights which exist for interconverting isomers Ia and Ib. The barrier heights for motion of the relatively weakly interacting CO molecule in resorcinol·CO should certainly be lower than those for water. It would be useful to conduct ab initio calculations to investigate how the potential-energy surfaces vary for the two clusters.

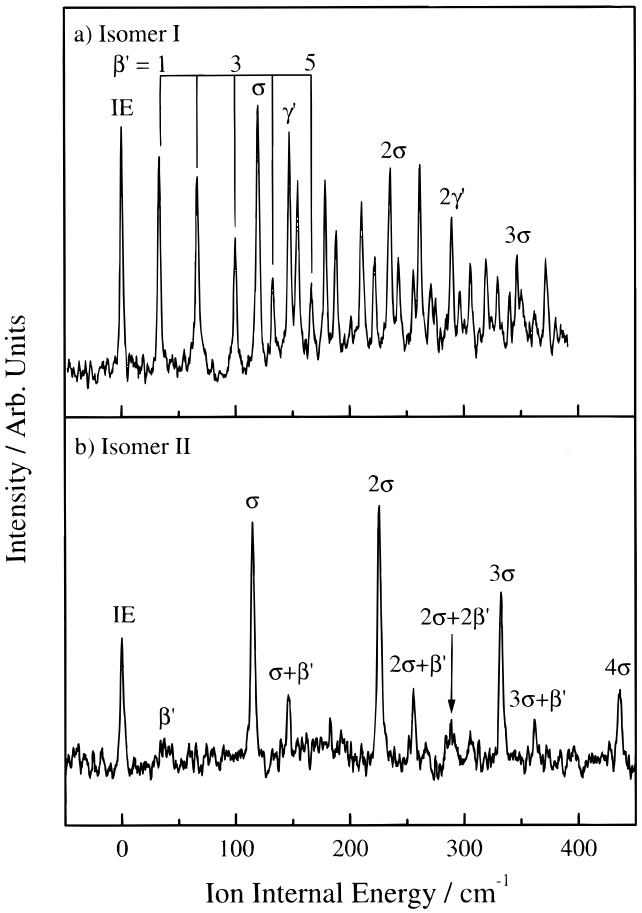

Figure 32. ZEKE spectra of resorcinol·CO recorded via the $S_1 0°$ state of (a) isomer I and (b) isomer II. Each spectrum is displayed relative to the respective ionization energy. Assignments of the in-plane bend (β'), in-plane wag (γ'), and intermolecular stretch (σ) modes are included on the spectra. (Reprinted with permission from ref 61. Copyright 1999 American Chemical Society.)

As in resorcinol·H_2O, the S_1-S_0 red shifts obtained from the REMPI spectrum (Figure 8a) were lower for the resorcinol·CO isomers (136 and 96 cm^{-1})[60] than for phenol·CO (190 cm^{-1}),[67] indicating comparatively weaker binding. The two rotational isomers can be associated with the rotational isomers of the monomer by consideration of these red shifts. ZEKE spectra were recorded via the respective $S_1 0°$ transitions for the two resorcinol·CO isomers and are displayed in Figure 32. The IEs of the isomers were determined as 65 293 (isomer I) and 65 702 (isomer II) cm^{-1}, which correspond to IE red shifts of 1404 and 1446 cm^{-1} (versus 1766 cm^{-1} for phenol·CO). While both spectra contain vibrational progressions of the β', γ', and σ intermolecular modes, the Franck–Condon patterns for excitation of these vibrations is remarkably different in the two systems. In particular, a strong progression in β' ($v = 1-5$) is observed for isomer I whereas even the single quanta of this mode is weak for isomer II. This suggests that substantially different geometry changes occur upon ionization from the S_1 intermediate state for the two isomers, an observation which is at odds with the ab initio calculations for the system, which indicate that

the intermolecular geometry is similar for both isomers in the S_0 and D_0 states. It is possible that the level of theory employed in the ab initio calculations is not sufficient, since CO possesses a small dipole moment which is notoriously difficult to calculate using HF and MP2 theory.

The resorcinol·H_2O and resorcinol·CO studies illustrate that a number of rotational isomers can be observed in a molecular beam expansion, identified, and therefore provided detailed information on how the environment of a solvent molecule is subtly different in a closely related series of compounds. The success of these experiments has led to the extension of this work to 3-methoxyphenol·H_2O complexes,[175] where it will be possible to compare the effect of an OCH_3 secondary functional group with the OH secondary group present in resorcinol.

V. Concluding Remarks

ZEKE and REMPI spectroscopy are excellent tools for characterizing molecular clusters due to their mass selectivity and the fact that typical spectral resolution allows low-frequency intermolecular vibrations to be readily resolved. This review has discussed the application of these methods to a wide range of complexes, from weakly bound vdW systems to hydrogen-bonded clusters. In this respect, the complexes of phenol with Ar, N_2, and CO are of particular interest since they illustrate the transition from vdW to hydrogen bonding. Ab initio calculations predict that each system should display stable vdW and hydrogen-bonding isomers, although the REMPI and ZEKE spectra of the complexes clearly demonstrate that only the vdW isomer is formed under supersonic jet conditions for phenol·Ar while only hydrogen-bonded isomers are formed for phenol·N_2 and phenol·CO. One of the current experimental challenges for spectroscopic research on molecular clusters is how to access the higher energy "missing" isomers in such systems. Such experiments are essential in order to more fully characterize the intermolecular potential-energy surface.

While the examples provided in this review illustrate that ZEKE spectroscopy is a powerful method for characterizing various cationic complexes, we note that there are certain systems where weak Franck−Condon intensity governs the ionization threshold region. This situation arises when large geometry changes occur for a molecule or complex upon ionization.[158,176−178] An example is provided by the 2-hydroxypyridine·H_2O complex,[176] which does not display a vibrationally resolved ZEKE spectrum. Ab initio calculations indicate that in the neutral complex, the water molecule binds via its oxygen atom to the hydroxyl group of the solute and with a hydrogen atom to the aromatic nitrogen atom. While the N···H interaction is attractive in the neutral complex, it becomes repulsive upon ionization since the excess positive charge is delocalized on the aromatic ring and induces a large intermolecular geometry change. A similar N···H interaction is present in phenol·$(NH_3)_n$ clusters.[177,178] However, the IR−UV techniques, within the constraints on accessible IR lasers, are not subject to this problem and therefore represent an excellent complement to ZEKE spectroscopy for studies of clusters which experience large geometry changes upon ionization.[79]

IR−UV and VIS−UV double-resonance spectroscopies clearly represent powerful spectroscopic schemes that will continue to be applied to a range of molecular clusters of current chemical interest. While most of the experiments to date have employed a combination of IR and UV photons, future experiments could exploit stimulated Raman transitions to study the spectroscopy of cationic clusters, in an SRS version of PIRI spectroscopy. This would extend the spectral range accessible with typical IR laser systems and would also extend the IR−UV schemes to complexes lacking strong IR transitions. In addition, it is clear that a combination of time-resolved measurements with double-resonance spectroscopies will provide a great deal of useful chemical information soon.

One of the most innovative recent applications of ZEKE spectroscopy is the work of Hepburn and coworkers[179,180] on Coulombic ion-pair states.[181] When excited to very high vibrational levels, these states resemble high-*n* Rydberg states and can be studied using pulsed field ionization techniques. It would be extremely interesting to extend this work to van der Waals[182] clusters since the threshold ion-pair production spectra should reveal the vibrational modes of the ion-pair potential-energy surface.

Another novel application of ZEKE spectroscopy is the recent work of Miller and co-workers on the organometallic complexes $CdCH_3$ and $Mg/ZnCH_3$.[183,184] These somewhat exotic "vdW" complexes are of interest not just due their practical relevance, e.g., $MgCH_3^+$ is a prototypical ionic intermediate of a Grignard reagent, but also due to the challenge they present to molecular orbital theories. It would certainly be useful to apply ZEKE spectroscopy to characterize the cationic states of a variety of other organometallic complexes such as cyclopentadiene−metal clusters.

Finally, we note that the further development of photoionization theories which allow the analysis of partially resolved rotational structure in ZEKE spectra should prove extremely useful for characterizing the structure of cationic complexes. The recent work of Wang et al.[113] has demonstrated an analysis of partially resolved rotational structure for the one-color nonresonant ZEKE spectrum of Na·H_2O. For the most widely used approach where ZEKE spectra are obtained via intermediate electronic states, it is necessary to determine of the rotational state population of the intermediate state as a function of the ground-state−intermediate-state transition wavenumber[185] prior to analyzing the partially resolved rotational structure of the cation.

VI. Acknowledgments

This work has been supported by grants from the Engineering and Physical Sciences Research Council (No. GR/L27770) and from the Joint Research Equipment Initiative 1998 (with P. J. Knowles, Birmingham, U.K.). C.E.H.D. gratefully acknowledges support from a Royal Society University Research

Fellowship. We thank Dr. Stephen Haines for assistance in preparing some of the figures used in this review and Gyorgy Tarczay for reading the manuscript and making useful suggestions.

VII. Note Added in Proof

A recent publication of Dopfer and co-workers (Solcà, N.; Dopfer, O. *Chem. Phys. Lett.* **2000**, *325*, 354) describes new results on the phenyl·Ar and phenol·N_2 cations discussed in this review. The cations are prepared by electron impact, which leads to the production of both a vdW and hydrogen-bonding cluster for [phenol·Ar]$^+$.

VIII. References

(1) Clausius, R. *Ann. Phys.* **1857**, *100*, 353.
(2) Maxwell, J. C. *Philos. Trans. R. Soc.* **1867**, *157*, 49.
(3) Boltzmann, L. *Sitz. Akad. Wiss., Wien* **1872**, *66*, 275.
(4) van der Waals, J. D. Ph. D Dissertation, Leiden, 1873.
(5) Müller-Dethlefs, K.; Hobza, P. *Chem. Rev.* **2000**, *100*, 143.
(6) Elrod, M. J.; Saykally, R. J.; Cooper, A. R.; Hutson, J. M. *Mol. Phys.* **1994**, *81*, 579.
(7) Fellers, R. S.; Leforestier, C.; Braly, L. B.; Brown, M. G.; Saykally, R. J. *Science* **1999**, 284, 945.
(8) Klopper, W.; Quack, M.; Suhm, M. A. *J. Chem. Phys.* **1998**, *108*, 10096.
(9) Klopper, W.; Quack, M.; Suhm, M. A. *Chem. Phys. Lett.* **1996**, *261*, 35.
(10) Chewter, L. A.; Müller-Dethlefs, K.; Schlag, E. W. *Chem. Phys. Lett.* **1987**, *135*, 219.
(11) Reiser, G.; Dopfer, O.; Lindner, R.; Henri, G.; Müller-Dethlefs, K.; Schlag, E. W.; Colson, S. D. *Chem. Phys. Lett.* **1991**, *181*, 1.
(12) Müller-Dethlefs, K.; Sander, M.; Schlag, E. W. *Z. Naturforsch. A* **1984**, *39*, 1089; *Chem. Phys. Lett.* **1984**, *112*, 291.
(13) Müller-Dethlefs, K.; Schlag, E. W. *Angew. Chem., Int. Ed. Engl.* **1998**, *37*, 1346.
(14) Müller-Dethlefs, K.; Dopfer, O.; Wright, T. G. *Chem. Rev.* **1994**, *94*, 1845.
(15) Müller-Dethlefs, K. *High-Resolution Photoionization and Photoelectron Studies*; Powis, I., Baer, T., Ng, C. Y., Eds.; J. Wiley & Sons Ltd: New York, 1995; p21.
(16) Cockett, M. C. R.; Müller-Dethlefs, K.; Wright, T. G. *Ann. Rep. R. Soc. Chem., Sect. C* **1998**, *94*, 327.
(17) Müller-Dethlefs, K.; Cockett, M. C. R. In *Nonlinear Spectroscopy for Molecular Structure Determination*; Blackwell Science: Oxford, England, 1998; Chapter 7.
(18) Müller-Dethlefs, K.; Schlag, E. W.; Grant, E. R.; Wang, K.; McKoy, B. V. *Advances in Chemical Physics XC*; Wiley: Chichester, England, 1995.
(19) Merkt, F. *Annu. Rev. Phys. Chem.* **1997**, *48*, 675.
(20) E. W. Schlag, *ZEKE Spectroscopy*; Cambridge University Press: Cambridge, 1998.
(21) Merkt, F.; Softley, T. P. *Int. Rev. Phys. Chem.* **1993**, *12*, 205.
(22) Beattie, D. A.; Donovan, R. J. *Prog. React. Kinet.* **1998**, *23*, 281.
(23) Johnson, P. M. *Acc. Chem. Res.* **1980**, *13*, 20.
(24) Parker; D. H.; Berg, J. O.; El-Sayed, M. A. In *Advances in Laser Chemistry*; Zewail, A. H., Ed.; Springer: New York, 1978.
(25) Nieman, G. C.; Colson, S. D. *J. Chem. Phys.* **1978**, *68*, 5656.
(26) Bernstein, R. B. *J. Phys. Chem.* **1986**, *100*, 32.
(27) Leutwyler, S.; Bosinger, J. *Chem. Rev.* **1990**, *90*, 489.
(28) Gruenloh, C. J.; Carney, J. R.; Arrington, C. A.; Zwier, T. S.; Fredericks, S. Y.; Jordan, K. D. *Science* **1997**, *276*, 1678.
(29) Barth, H.-D.; Buchhold, K.; Djafari, S.; Reimann, B.; Lommatzsch, U.; Brutchy, B. *Chem. Phys.* **1998**, *239*, 49.
(30) Janzen, Ch.; Spangenberg, D.; Roth, W.; Kleinermanns, K. *J. Chem. Phys.* **1999**, *110*, 9898.
(31) Haines, S. R.; Geppert, W. D.; Chapman, D. M.; Watkins, M. J.; Dessent, C. E. H.; Cockett, M. C. R.; Müller-Dethlefs, K. *J. Chem. Phys.* **1998**, *109*, 9244.
(32) Boesl, U.; Weinkauf, R.; Schlag, E. W. *Int. J. Mass Spectrom. Ion Processes* **1992**, *112*, 1992.
(33) Neusser, H. J.; Krause, H. *Chem. Rev.* **1994**, *94*, 1829.
(34) Helm, R. M.; Vogel, H.-P.; Neusser, H. J. *J. Chem. Phys.* **1998**, *108*, 4496.
(35) Pratt, D. W. *Annu. Rev. Phys. Chem.* **1998**, *49*, 481.
(36) Berden, G.; Meerts, W. L.; Schmitt, M.; Kleinermanns, K. *J. Chem. Phys.* **1996**, *104*, 972.
(37) Turner, D. W.; Al Joboury, M. I. *J. Chem. Phys.* **1962**, *37*, 3007.
(38) Turner, D. W.; Baker, C.; Baker, A. D.; Brundle, C. R. *Molecular Photoelectron Spectroscopy*; Academic Press: New York, 1979.
(39) Martensson, N.; Baltzer, P.; Bruhwiler, P. A.; Forsell, J. O.; Nilsson, A. Stenborg, A.; Wannberg, B. *J. Electron. Spectrosc. Relat. Phenom.* **1994**, *70*, 117. Szepes, L.; Tarczay, G. In *Encyclopedia of Spectroscopy and Spectrometry*; 1999.
(40) Villarejo, D.; Herm, R. R.; Inghram, M. G. *J. Chem. Phys.* **1967**, *46*, 4995.
(41) Peatman, W. B.; Borne, T. B.; Schlag, E. W. *Chem. Phys. Lett.* **1969**, *3*, 492.
(42) Dietrich, H.-J.; Müller-Dethlefs, K.; Baranov, L. Ya *Phys. Rev. Lett.* **1996**, *76*, 3530.
(43) Freund, R. S. *J. Chem. Phys.* **1971**, *54*, 3125.
(44) Chupka, W. A. *J. Chem. Phys.* **1993**, *98*, 4520; *ibid* **1993**, *99*, 5800.
(45) Merkt, F.; Xu, H.; Zare, R. N. *J. Chem. Phys.* **1996**, *104*, 950.
(46) Baranov, L. Ya; Held, A.; Selzle, H. L.; Schlag, E. W. *Chem. Phys. Lett.* **1998**, *291*, 311.
(47) Held, A.; Baranov, L. Ya; Selzle, H. L.; Schlag, E. W. *Chem. Phys. Lett.* **1998**, *291*, 318.
(48) Fischer, I.; Lindner, R.; Müller-Dethlefs, K. *J. Chem. Soc., Faraday Trans.* **1994**, *90*, 2425.
(49) Lindner, R.; Dietrich, H.-J.; Müller-Dethlefs, K. *Chem. Phys. Lett.* **1994**, *228*, 417.
(50) Dessent, C. E. H.; Haines, S. R.; Müller-Dethlefs, K. *Chem. Phys. Lett.*, **1999**, *315*, 103.
(51) Dietrich, H.-J.; Lindner, R.; Müller-Dethlefs, K. *J. Chem. Phys.* **1994**, *101*, 3399.
(52) Lipert, R. J.; Colson, S. D. *J. Phys. Chem.* **1989**, *93*, 15.
(53) Scherzer, W.; Selzle, H. L.; Schlag, E. W. *Chem. Phys. Lett.* **1992**, *195*, 11.
(54) Benhorin, N.; Even, U.; Jortner, J. *Chem. Phys. Lett.* **1992**, *188*, 73.
(55) Fernandez, J. A.; Yao, J.; Bernstein, E. R. *J. Chem. Phys.* **1999**, *110*, 5159; *ibid* **1999**, *110*, 5174.
(56) Hamabe, H.; Fukuchi, T.; Shiraishi, S.; Nishi, K.; Nishimura, Y.; Tsuji, T.; Nishi, N.; Sekiya, H. *J. Phys. Chem. A* **1998**, *102*, 3880.
(57) Gerhards, M.; Perl, W.; Kleinermanns, K. *Chem. Phys. Lett.* **1995**, *240*, 506.
(58) Graham, R. J.; Kroemer, R. T.; Mons, M.; Robertson, E. G.; Snoek, L. C.; Simons, J. P. *J. Phys. Chem. A* **1999**, *103*, 9706.
(59) Bach, A.; Hewel, J.; Leutwyler, S. *J. Phys. Chem. A* **1998**, *102*, 10476.
(60) Geppert, W. D.; Dessent, C. E. H.; Ullrich, S.; Müller-Dethlefs, K. *J. Phys. Chem. A* **1999**, *103*, 7186.
(61) Geppert, W. D.; Dessent, C. E. H.; Müller-Dethlefs, K. *J. Phys. Chem. A* **1999**, *103*, 9687.
(62) Le Barbu, K.; Brenner, V.; Millie, Ph; Lahmani, F.; Zehnacker-Rentien, A. *J. Phys. Chem. A* **1998**, *102*, 128.
(63) Satta, M.; Latini, A.; Piccirillo, S.; DiPalma, T. M.; Scuderi, D.; Speranza, M.; Giardini, A. *Chem. Phys. Lett.* **2000**, *316*, 94.
(64) Haines, S. R.; D. Phil Dissertation, Univeristy of York, 1999.
(65) Chapman, D. M.; Hompf, F. J.; Müller-Dethlefs, K.; Waterstradt, E.; Hobza, P.; Spirko, V. *Chem. Phys.* **1998**, *239*, 417.
(66) Zhu, L.; Johnson, P. *J. Chem. Phys.* **1991**, *94*, 5769.
(67) Haines, S. R.; Dessent, C. E. H.; Müller-Dethlefs, K. *J. Chem. Phys.*, **1999**, *111*, 1947.
(68) Lembach, G.; Brutschy, B. *J. Phys. Chem.* **1996**, *100*, 19758.
(69) Pitts, J. D.; Knee, J. L. *J. Chem. Phys.* **1998**, *109*, 7113.
(70) Grebner, Th. L.; Unold, P. v.; Neusser, H. *J. Phys. Chem. A* **1997**, *101*, 158.
(71) Taylor, D. P.; Goode, J. G.; LeClaire, J. E.; Johnson, P. M. *J. Chem. Phys.* **1995**, *103*, 6293.
(72) Anand, R.; LeClaire, J. E.; Johnson, P. M. *J. Phys. Chem. A* **1999**, *103*, 2618.
(73) Fujii, A.; Iwasaki, A.; Ebata, T.; Mikami, N. *J. Phys. Chem. A* **1997**, *101*, 5963.
(74) Gerhards, M.; Schiwek, Unterberg, C.; Kleinermanns, K. *Chem. Phys. Lett.* **1998**, *297*, 515.
(75) Cooper, D. E.; Klimcak, C. M.; Wessel, J. E. *Phys. Rev. Lett.* **1981**, *46*, 324.
(76) Syage, J. A.; Wessel, J. E. *Appl. Opt.* **1987**, *26*, 3573.
(77) Murakami, J.; Kaya, K.; Ito, M. *Chem. Phys. Lett.* **1982**, *91*, 401.
(78) Gruenloh, C. J.; Hagemeister, F. C.; Carney, J. R.; Zwier, T. S. *J. Phys. Chem. A* **1999**, *103*, 503.
(79) Kleinermanns, K.; Janzen, Ch.; Spangenberg, D.; Gerhards, M. *J. Phys. Chem. A* **1999**, *103*, 5239.
(80) Fujii, A.; Miyazaki, M.; Ebata, T.; Mikami, N. *J. Chem. Phys.* **1999**, *110*, 1125.
(81) Piest, H.; von Helden, G.; Meijer, G. *J. Chem. Phys.* **1999**, *110*, 2010.
(82) Satink, R. G.; Piest, H.; Helden, G. v.; Meijer, G. *J. Chem. Phys.* **1999**, *111*, 10750.
(83) Riehn, Ch.; Lahmann, Ch.; Wassermann, B.; Brutschy, B. *Ber. Bunsen-Ges. Phys. Chem.* **1992**, *96*, 1161.
(84) Djafari, S.; Barth, H.-D.; Buchold, K.; Brutschy, B. *J. Chem. Phys.* **1997**, *107*, 10573.
(85) Felker, P. M.; Maxton, P. M.; Schaeffer, M. W. *Chem. Rev.* **1994**, *94*, 1721.

(86) Ishikawa, S.; Ebata, T.; Ishikawa, H.; Inoue, T.; Mikami, N. *J. Phys. Chem.* **1996**, *100*, 10531.
(87) Kim, W.; Schaeffer, M. W.; Lee, S.; Chung, J. S.; Felker, P. M. *J. Chem. Phys.* **1999**, *110*, 11264.
(88) Pitts, J. D.; Knee, J. L. *J. Chem. Phys.* **1999**, *110*, 3389.
(89) Zhang, X.; Pitts, J. D.; Nadarajah, R.; Knee, J. L. *J. Chem. Phys.* **1999**, *110*, 3389.
(90) Lembach, G.; Brutschy, B. *J. Phys. Chem. A* **1998**, *102*, 6068.
(91) Syage, J. A. *J. Phys. Chem.* **1995**, *99*, 5772. Steadman, J. A.; Syage, J. A. *J. Phys. Chem.* **1991**, *95*, 10326.
(92) Kim, S. K.: Breen, J. J.; Willberg, D. M.; Peng, L. W.; Heikal, A.; Syage, J. A.; Zewail, A. H. *J. Phys. Chem.* **1995**, *99*, 7421.
(93) Pino, G.; Gregoire, G.; Dedonder-Lardeux, C.; Jouvet, C.; Martrenchard, S.; Solgadi, D. *Phys. Chem. Chem. Phys.* **2000**, *2*, 893.
(94) Folmer, D. E.; Wisniewski, E. S.; Castlemann, A. W. *Chem. Phys. Lett.* **2000**, *318*, 637.
(95) Colbourn, A. E.; Douglas, E. A. *J. Chem. Phys.* **1976**, *65*, 1741.
(96) Dehmer, P. M.; Dehmer, J. L. *J. Chem. Phys.* **1978**, *69*, 125.
(97) Signorell, R.; Merkt, F. *J. Chem. Phys.* **1998**, *109*, 9762.
(98) Bush, A. M.; Dyke, J. M.; Mack, P.; Smith, D. M.; Wright, T. G. *J. Chem. Phys.* **1998**, *108*, 406.
(99) Barr, J. D.; Dyke, J. M.; Mack, P.; Smith, D. M.; Wright, T. G. *J. Electron. Spectrosc. Relat. Phenom.* **1998**, 97, 159.
(100) Cockett, M. C. R. *J. Electron. Spectrosc. Relat. Phen.* **1998**, *97*, 171.
(101) Beattie, D. A.; Cockett, M. C. R.; Lawley, K. P.; Donovan, R. J. *J. Chem. Soc., Farady Trans.* **1997**, *93*, 4245.
(102) Hutson, J. M. *Adv. Mol. Vib. Collision Dyn.* **1991**, *1*, 1.
(103) Fischer, I.; Strobel, A.; Staecker, J.; Niedner-Schattenurg, G.; Müller-Dethlefs, K. *J. Chem. Phys.* **1992**, *96*, 7171.
(104) Strobel, A.; Knoblauch, N.; Agreiter, J.; Smith, A. M.; Niedner-Scatteburg, G.; Bondybey, V. E. *J. Phys. Chem.* **1995**, *99*, 872.
(105) Urban, B.; Strobel, A.; Bondybey, V. E. *J. Chem. Phys.* **1999**, *111*, 8939.
(106) Lee, E. P. F.; Wright, T. G. *Chem. Phys. Lett.* **1999**, *301*, 467.
(107) East, A. L. L.; Watson, J. K. G. *J. Chem. Phys.* **1999**, *110*, 6099.
(108) Farmanara, P.; Radloff, W.; Stert, V.; Ritze, H.-H.; Hertel, I. V. *J. Chem. Phys.* **1999**, *111*, 633.
(109) Kamke, W.; Hermann, R.; Wang, W.; Hertel, I. V. *Z. Phys. D* **1988**, *10*, 491.
(110) Glendening, E. D. *J. Am. Chem. Soc.* **1996**, *118*, 2473.
(111) Schulz, C. P.; Haugstatter, R.; Tttes, H. U.; Hertel, I. V. *Phys. Rev. Lett.* **1986**, *57*, 1703.
(112) Rodham, D. A.; Blake, G. A. *Chem. Phys. Lett.* **1997**, *264*, 522.
(113) Wang, K. H.; Rodham, D. A.; McKoy, V.; Blake, G. A. *J. Chem. Phys.* **1998**, *108*, 4817.
(114) Beswick, J. A.; Jortner, J. *Adv. Chem. Phys.* **1981**, *47*, 263.
(115) Castleman, A. W.; Keesee, R. G. *Annu. Rev. Phys. Chem.* **1986**, *37*, 525.
(116) Menapace, J. A.; Bernstein, E. R. *J. Phys. Chem.* **1987**, *91*, 2533.
(117) Benhorin, N.; Even, U.; Jortner, J. *J. Chem. Phys.* **1989**, *1*, 331.
(118) Neusser, H. J.; Krause, H. *Chem. Rev.* **1994**, *94*, 1829.
(119) Amirav, A.; Even, U.; Jortner, J.; Dick, B. *Mol. Phys.* **1983**, *49*, 899.
(120) Weber, Th.; Riedle, E.; Neusser, H. J.; Schlag, E. W. *Chem. Phys. Lett.* **1991**, *183*, 77.
(121) Lembach, G.; Brutschy, B. *Chem. Phys. Lett.* **1997**, *273*, 421.
(122) Lembach, G.; Brutschy, B. *J. Chem. Phys.* **1997**, *107*, 6156.
(123) Pitts, J. D.; Knee, J. L. *J. Chem. Phys.* **1999**, *110*, 3389.
(124) Benhorin, N.; Even, U.; Jortner, J. *Chem. Phys. Lett.* **1992**, *188*, 73.
(125) Tanaka, D.; Sato, S.; Kimura, K. *Chem. Phys.* **1998**, *239*, 437.
(126) Inoue, H.; Sato, S.; Kimura, K. *J. Electron. Spectrosc. Relat. Phenom.* **1998**, *88*, 125.
(127) Hobza, P.; Selzle, H. L.; Schlag, E. W. *J. Chem. Phys.* **1991**, *95*, 391.
(128) Hobza, P.; Bludsky, D.; Selzle, H. L.; Schlag, E. W. *Chem. Phys. Lett.* **1996**, *250*, 402.
(129) Koch, H.; Fernandez, B.; Christiansen, O. *J. Chem. Phys.* **1998**, *108*, 2784.
(130) Mons, M.; Le Calve, *J. Chem. Phys.* **1990**, *146*, 195.
(131) Ullrich, S. et al. Manuscript in preparation.
(132) Chapman, D. M. D. Phil Dissertation, University of York, 1999.
(133) Haines, S. R.; Dessent, C. E. H.; Müller-Dethlefs, K. *J. Electron. Spectrosc. Relat. Phenom.* **2000**, *108*, 1.
(134) Bieske, E. J.; Rainbird, M. W.; Atkinson, I. M.; Knight, A. E. W. *J. Chem. Phys.* **1989**, *91*, 752.
(135) Zhang, X.; Knee, J. L. *Faraday Discuss.* **1994**, *97*, 299.
(136) Lombardi, J. R. *J. Chem. Phys.* **1969**, *50*, 3780.
(137) Zhang, X.; Smith, J. M.; Knee, J. L. *J. Chem. Phys.* **1992**, *97*, 2843.
(138) Leopold, K. R.; Fraser, G. T.; Novick, S. E.; Klemperer, W. *Chem. Rev.* **1994**, *94*, 1807.
(139) Jeriorski, B.; Moszynski, R.; Szalewicz, K. *Chem. Rev.* **1994**, *94*, 1887.
(140) Oikawa, A.; Abe, H.; Mikami, N.; Ito, M. *J. Phys. Chem.* **1983**, *87*, 5083.
(141) Lipert, R. J.; Colson, S. D. *J. Chem. Phys.* **1988**, *89*, 4579.
(142) Nowak, R.; Manapace, J. A.; Bernstein, E. R. *J. Chem. Phys.* **1997**, *101*.
(143) Weber, T.; Smith, A. M.; Riedle, E.; Neusser, H. J.; Schlag, E. W. *Chem. Phys. Lett.* **1990**, *175*, 79.
(144) Shinohara, H.; Ikeda, K.; Kimura, K. *J. Electron. Spectrosc. Relat. Phenom.* **1998**, *88*, 131.
(145) Chapman, D. M.; Müller-Dethlefs, K.; Peel, J. B. *J. Chem. Phys.* **1999**, *111*, 1955.
(146) Jackel, J. G.; Jones, H. *Chem. Phys.* **1999**, *247*, 321.
(147) Sinha, H.; Steer, R. P. *Chem. Phys. Lett.* **1995**, *241*, 328.
(148) Dopfer, O.; Reiser, G.; Müller-Dethlefs, K.; Schlag, E. W.; Colson, S. *J. Chem. Phys.* **1994,** *101*, 974.
(149) Hu, Y.; Lu, W.; Yang, S. *J. Chem. Phys.* **1996**, *105*, 5305.
(150) Graham, C.; Impie, D. A.; Raab, R. E. *Mol. Phys.* **1998**, *93*, 49.
(151) Braun, J. E.; Grebner, Th. L.; Neusser, H. J. *J. Phys. Chem. A* **1998**, *102*, 3373.
(152) Hockridge, M. R.; Knight, S. M.; Robertson, E. G.; Simons, J. P.; McCombie, J.; Walker, M. *Phys. Chem. Chem. Phys.* **1999**, 1, 407.
(153) Dickinson, J. A.; Hockridge, M. R.; Kroemer, R. T.; Robertson, E. G.; Simons, J. P.; McCombie, J.; Walker, M. *J. Am. Chem. Soc.* **1998**, *120*, 2622.
(154) Dickinson, J. A.; Joireman, P. W.; Randall, R. W.; Robertson, E. G.; Simons, J. P. *J. Phys. Chem. A* **1997**, *101*, 513.
(155) Kromer, R. T.; Liedl, K. R.; Dickinson, J. A.; Robertson, E. G.; Simons, J. P.; Borst, D. R.; Pratt, D. W. *J. Am. Chem. Soc.* **1998**, *120*, 12573.
(156) Phillips, L. A.; Levy, D. H. *J. Chem. Phys.* **1988**, *89*, 85.
(157) Hopkins, J. B.; Powers, D. E.; Smalley, R. E. **1980**, *72*, 5039.
(158) Dessent, C. E. H.; Geppert, W. D.; Ullrich, S.; Müller-Dethlefs, K. *Chem. Phys. Lett.* **2000**, 319, 375.
(159) Dopfer, O.; Lembach, G.; Wright, T. G.; Müller-Dethlefs, K. *J. Chem. Phys.* **1993**, *98*, 1933.
(160) Pribble, R. N.; Hagemeister, F. C.; Zwier, T. S. *J. Chem. Phys.* **1997**, *106*, 2145.
(161) Gruenloh, C. J.; Florio, G. M.; Carney, J. R.; Hagemeister, F. C.; Zwier, T. S. *J. Phys. Chem. A* **1999**, *103*, 496.
(162) Carney, J. R.; Hagemeister, F. C.; Zwier, T. S. *J. Chem. Phys.* **1998**, *108*, 3379.
(163) Janzen, Ch.; Spangenberg, D.; Roth, W.; Kleinermanns, K. *J. Chem. Phys.* **1999**, *110*, 9898,
(164) Graham, R. J.; Kroemer, R. T.; Mons, M.; Robertson, E. G.; Snoek, L. C.; Simons, J. P. *J. Phys. Chem. A* **1999**, *103*, 9706.
(165) Guchait, N.; Ebata, T.; Mikami, N. *J. Chem. Phys.* **1999**, *111*, 8438.
(166) Mitsui, M.; Ohshima, Y.; Ishiuchi, S.; Sakai, M.; Fujii, M. *Chem. Phys. Lett.* **2000**, *317*, 211. Yoshino, R.; Hashimoto, K.; Omi, T.; Ishiuchi, S.; Fujii, M. *J. Phys. Chem. A* **1998**, *102*, 6227.
(167) Wanna, J.; Menapace, J. A.; Bernstein, E. R. *J. Chem. Phys.* **1986**, *85*, 1795.
(168) Hineman, M. F.; Brucker, G. A.; Kelley, D. F.; Bernstein, E. R. *J. Chem. Phys.* **1992**, *97*, 3341.
(169) Gerhards, M.; Perl, W.; Kleinermanns, K. *Chem. Phys. Lett.* **1995**, *240*, 506.
(170) Gerhards, M.; Schumm, S.; Uterberg, C.; Kleinermanns, K. *Chem. Phys. Lett.* **1998**, *294*, 65.
(171) Gerhards, M.; Uterberg, C.; Schumm, S. *J. Chem. Phys.* **1999**, *111*, 7966.
(172) Melandri, S.; Maccaferri, G.; Caminati, W.; Favero, P. G. *Chem. Phys. Lett.* **1996**, *256*, 513.
(173) Hobza, P.; Burcl, R.; Spirko, V.; Dopfer, O.; Müller-Dethlefs, K.; Schlag, E. W. *J. Chem. Phys.* **1994,** *101*, 990.
(174) Dopfer, O.; Lembach, G.; Wright, T. G.; Müller-Dethlefs, K. *J. Chem. Phys.* **1993**, *98*, 1933.
(175) Geppert, W. D.; Ullrich, S.; Dessent, C. E. H.; Müller-Dethlefs, K. *J. Phys. Chem. A*, submitted for publication.
(176) Geppert, W. D. D. Phil. Dissertation, University of York, 1999.
(177) Jacoby, C.; Hering, P.; Schmitt, M.; Roth, W.; Kleinermanns, K. *Chem. Phys.* **1998**, *239*, 23 and references therein.
(178) Pino, G. A.; Dedonder-Lardeux, C.; Gregoire, G.; Jouvet, C.; Martrenchard, S.; Solgadi, D. *J. Chem. Phys.* **1999**, *111*, 10747.
(179) Martin, J. D. D.; Hepburn, J. W. *Phys. Rev. Lett.* **1997**, *79*, 3154.
(180) Martin, J. D. D.; Hepburn, J. W. *J. Chem. Phys.* **1998**, *109*, 8139.
(181) Lawley, K. P.; Donovan, R. J. *J. Chem. Soc., Faraday Trans.* **1993**, *89*, 1885.
(182) Geppert, W. D.; Dessent, C. E. H.; Cockett, M. C. R.; Müller-Dethlefs, K. *Chem. Phys. Lett.* **1999**, *303*, 194.
(183) Panov, S. I.; Powers, D. E.; Miller, T. A. *J. Chem. Phys.* **1998**, *108*, 1335.
(184) Barckholtz, T. A.; Powers, D. E.; Miller, T. A.; Bursten, B. E. *J. Am. Chem. Soc.* **1999**, *121*, 2576.
(185) Ford, M. S.; Haines, S. R.; Pugliesi, I.; Dessent, C. E. H.; Müller-Dethlefs, K. *J. Electron. Spectrosc. Relat. Phenom.*, in press.

CR990060R